3-2021

# Cyclic Pursuit

Daniel E. Oke


# CYCLIC PURSUIT

THESIS

Daniel E Oke, B.S.C.S, TSgt, USAF

AFIT-ENG-MS-21-M-068

**DEPARTMENT OF THE AIR FORCE**
**AIR UNIVERSITY**

***AIR FORCE INSTITUTE OF TECHNOLOGY***

**Wright-Patterson Air Force Base, Ohio**

AFIT-ENG-MS-21-M-068

# CYCLIC PURSUIT

THESIS

Presented to the Faculty

Department of Electrical and Computer Engineering

Graduate School of Engineering and Management

Air Force Institute of Technology

Air University

Air Education and Training Command

in Partial Fulfillment of the Requirements for the

Degree of Master of Science in Computer Science

Daniel E Oke, B.S.C.S, B.S.C.S

TSgt, USAF

March 25, 2021

AFIT-ENG-MS-21-M-068

# CYCLIC PURSUIT

THESIS

Daniel E Oke, B.S.C.S, B.S.C.S
TSgt, USAF

Committee Membership:

Meir Pachter, Ph.D
Chair

Major. Jorge J Betances, Ph.D
Member

Robert C Leishman, Ph.D
Member

AFIT-ENG-MS-21-M-068

# Abstract

This thesis analyzes cyclic pursuit with the intent of developing swarm attack strategies for autonomous agents. Research was focused on finding the effects of pursuers capture range, evader speed and size of formation on the probability of escape. The temporal evolution of several polygonal formations was analyzed. The polygons could be regular or arbitrary polygons. The thesis demonstrated that an increased capture range, formation size, reduced evader speed aided capture probability. Irregular n-gon formations reduced to n-1 gon repeatedly, pursuer clusters formed until two clusters remained which eventually came together, so all the n pursuers coalesced until convergence. Regular n-gon polygon formation maintained their form until coalesced. Sufficient conditions for the capture of the evader are provided at the end of the analysis.

# Table of Contents

Page

# List of Figures

Figure Page

# List of Tables

CYCLIC PURSUIT

# I. Introduction

## 1.1 Introduction

Pursuit evasion is a known set of problems in computer science and mathematics in which a group attempts to capture another group within certain defined parameters. Pursuit evasion problems have a long history. It dates back to the 1700s when problems of pirates chasing merchant ships in the high seas were a thing. In the twentieth century, game theory re-emerged as the mathematical tool that was employed to formalize or solve these problems. Pursuit evasion (multi-player) scenarios are where a group of $N$ pursuers strives to co-operatively capture a surrounded evader. In this study the pursuers employ cyclic pursuit, that is, 'Pursuer $I$' is in pure pursuit of 'Pursuer $I+1$' and the loop is closed by the 'Pursuer $N$' who is after 'Pursuer 1' (see Figure 1). Cyclic pursuit causes the pursuer's formation to shrink in a cyclical form and eventually ensnarl the evader [1, 2, 3, 4, 5].Cyclic pursuit goes beyond computer science and mathematics -we see it every day. Many scientists believe its knowledge helps uncover laws of nature, and unravel the laws of the universe [6].

Capturing an evader in a cyclic pursuit is an intriguing pursuit evasion problem. While the intent of this thesis is to develop swarm attack strategies for autonomous agent, cyclic pursuit is being proposed in several areas of technology and research today. Such areas include capturing in 3D space [1], bearing-only angles measurement based cyclic pursuit [2], creature behavior based cyclic pursuit [7], perimeter tracking by multiple UAVs [8, 9, 10] and application of cyclic pursuit to formation

reconfiguration [11], to mention a few .

Cyclic pursuit curves originate from the mathematics of pursuit curves and keeps agents (pursuers) formation in collective, uniform distribution and re-orientation. Cyclic pursuit strategy resides in interaction based on local information, therefore it does not have the problem of time delay, large information payload or other disturbances that may prevent global convergence.[11]

The advantages of cyclic pursuit can be concluded as follows. First, it requires less communication exchange: it just needs the relative measurement of position and velocity. Second, no leader agent or pursuer is required in the formation; making it a decentralized control scheme. Such agent formations have stronger anti-disturb and refresh ability. [11, 7, 12, 13]

### 1.2 Previous work and Research Objectives

Some previous work has been done in cyclic pursuit. Lin was able to show that stable multipe pursuers will eventually converge to a single point. He explained that when agents are arranged in counter clockwise or clockwise star formation, the remain unchanged and therefore no collison [14]. Sinha studied the case where speeds and controller gains for the agents where varied, thus a heterogenus system. Sinha determined the conditions in which convergence would occur [15]. Kim proposed a method in 3D space involving co-operative target capturing using cyclic pursuit strategy. Kim considers a group of n pursuers dispersed in a 3D space. Next, develops a distributed controller based on modified cyclic pursuit methodology. Using simple and local information, the control achieves the desired global behaviour of the agents [1]. The objective of this research is in four parts. First, evaluating the relationship between the capture range of the pursuer and the speed of the evader. This analysis

is conducted while the evader escapes by selecting several routes in the formation. Second, evaluating the evolution of the distances between neighbouring pursuers in a triangular formation during cyclic pursuit while studying the location of the vertex angle formed for each isosceles formation. Third, determining a closed form solution for capturability in given formation. Finally, an analysis focused on the evolution of formations for regular and irregular polygons. In all cases, the pursuers have the same velocity and each pursuer has information of the current location of the pursuer immediately ahead. Evader and pursuers exist only in the 2D space.

### 1.3 Document Overview

The Introduction section highlights the previous work/research that has been done in this area and its advantages over other alternatives. The Background and Literature Review section elaborates on the dynamics building upto the four pursuers and one evader scenarios. The equations are introduced in such a way to allow for Euler theory for simulation/animation. The Methodology section first discusses the topic on Regions of Capturability. This talks about how the evader can select escape cones and various ways of doing so. Temporal Evolution of Distances of the pursuers over a specified time was studied also discussed in this section. The evolution of pursuer formation size for several polygon formation was studied. Lastly, for a triangle formation, capturability was derived in terms of mathematical equations given certain parameters. The equations were validated in several simulations. The Results section elaborated on the findings from the simulations conducted in the methodology section. The conclusion section gave a summary of all the findings and any future work.

# II. Background and Literature Review

## 2.1 Background and Literature Review

### 2.1.1 Two Pursuers

Consider the simplest cyclic pursuit scenario were only two pursuers, $P_1$ and $P_2$ are at work. $P_1$ runs toward $P_2$ and at the same time $P_2$ runs toward $P_1$. Obviously, the pursuit evolves along a straight line and if the initial distance between the pursuers is r and the speed of the pursuers is 1 they will coalesce/meet at time $t_f = \frac{r}{2}$ – we have a "train wreck".

But we want to simulate this situation in general position. Thus, let the position of $P_1$ in the Euclidean plane be $(x_1, y_1)$; the initial position in the Euclidean plane of $P_1$ is $(x_{1_0}, y_{1_0})$. The position of $P_2$ in the Euclidean plane is $(x_2, y_2)$ and the initial position of $P_2$ in the Euclidean plane is $(x_{2_0}, y_{2_0})$. There are four states: $(x_1, y_1, x_2, y_2)$. Must determine the time histories $(x_1(t), y_1(t), x_2(t), y_2(t))$, $0 \leq t \leq t_f$ where

$$t_f = \frac{1}{2}\sqrt{(x_{2_0} - x_{1_0})^2 + (y_{2_0} - y_{1_0})^2} \tag{1}$$

Because $P_1$ runs toward $P_2$ and his speed is 1, the continuous-time dynamics are

$$\frac{dx_1}{dt} = \frac{x_2 - x_1}{\sqrt{(x_2 - x_1)^2 + (y_2 - y_1)^2}},\ x_1(0) = x_{1_0} \tag{2}$$

$$\frac{dy_1}{dt} = \frac{y_2 - y_1}{\sqrt{(x_2 - x_1)^2 + (y_2 - y_1)^2}},\ y_1(0) = y_{1_0} \tag{3}$$

Because $P_2$ runs toward $P_1$ and his speed is 1, the continuous-time dynamics are

$$\frac{dx_2}{dt} = \frac{x_2 - x_1}{\sqrt{(x_2 - x_1)^2 + (y_2 - y_1)^2}},\ x_2(0) = x_{2_0} \tag{4}$$

$$\frac{dy_2}{dt} = \frac{y_2 - y_1}{\sqrt{(x_2 - x_1)^2 + (y_2 - y_1)^2}},\ y_2(0) = y_{2_0},\quad 0 \le t \le t_f \tag{5}$$

Using the Euler integration scheme:

$$x_1(t + dt) = x_1(t) + \frac{x_2 - x_1}{\sqrt{(x_2 - x_1)^2 + (y_2 - y_1)^2}}dt,\ x_1(0) = x_{1_0} \tag{6}$$

$$y_1(t + dt) = y_1(t) + \frac{y_2 - y_1}{\sqrt{(x_2 - x_1)^2 + (y_2 - y_1)^2}}dt,\ y_1(0) = y_{1_0} \tag{7}$$

$$x_2(t + dt) = x_2(t) + \frac{x_1 - x_2}{\sqrt{(x_2 - x_1)^2 + (y_2 - y_1)^2}}dt,\ x_2(0) = x_{2_0} \tag{8}$$

$$\begin{aligned} y_2(t + dt) = y_2(t) + \frac{y_1 - y_2}{\sqrt{(x_2 - x_1)^2 + (y_2 - y_1)^2}}dt, \\ y_2(0) = y_{2_0}, t = 0, dt, 2dt, 3dt, ...t_f \end{aligned} \tag{9}$$

### 2.1.2 Three Pursuers

We now introduce the third Pursuer $P_3$ whose instantaneous position is $(x_3, y_3)$; the initial position of $P_3$ is $(x_{3_0}, y_{3_0})$. The three Pursuers are located at the vertices of $\triangle\ P_1P_2P_3$.

As before $P_1$ goes after $P_2$, so eqs. (2), (3), and consequently, the Euler integration

scheme's eqs. (6) and (7), are unchanged.

But now $P_2$ goes after $P_3$ so eqs. (4) and (5) are replaced by

$$\frac{dx_2}{dt} = \frac{x_3 - x_2}{\sqrt{(x_3 - x_2)^2 + (y_3 - y_2)^2}},\ x_2(0) = x_{2_0} \tag{10}$$

$$\frac{dy_2}{dt} = \frac{y_3 - y_2}{\sqrt{(x_3 - x_2)^2 + (y_3 - y_2)^2}},\ y_2(0) = y_{2_0},\quad 0 \le t \le t_f \tag{11}$$

The Euler integration scheme's eqs. (8) and (9) must be changed accordingly.

Finally, the new Pursuer $P_3$ "closes the loop" by going after $P_1$ and the additional dynamics are

$$\frac{dx_3}{dt} = \frac{x_1 - x_3}{\sqrt{(x_3 - x_1)^2 + (y_3 - y_1)^2}},\ x_3(0) = x_{3_0} \tag{12}$$

$$\frac{dy_3}{dt} = \frac{y_1 - y_3}{\sqrt{(x_3 - x_1)^2 + (y_3 - y_1)^2}},\ y_3(0) = y_{3_0},\quad 0 \le t \le t_f \tag{13}$$

A new set of two Euler equations is needed for the numerical integration of the dynamics (2), (3), (9)-(12).

Now $t_f$ will not be determined by eq. (1) but will be determined by the condition

$$\begin{aligned}(x_2 - x_1)^2 + (y_2 - y_1)^2 + (x_3 - x_2)^2 + (y_3 - y_2)^2 \\ +(x_3 - x_1)^2 + (y_3 - y_1)^2 = \epsilon^2\end{aligned} \tag{14}$$

where $\epsilon = 1 \cdot dt$.

### 2.1.3 Four Pursuers

In this case, the position of the fourth Pursuer $P_4$ is $(x_4, y_4)$. Equations (2), (3), (10), (11) are unchanged. In eqs. (12) and (13) replace $x_1$ with $x_4$ and $y_1$ with $y_4$; the Euler integration scheme equations need to be changed accordingly. Finally, the new Pursuer $P_4$ "closes the loop" by going after $P_1$ and the additional dynamics are

$$\frac{dx_4}{dt} = \frac{x_1 - x_4}{\sqrt{(x_4 - x_1)^2 + (y_4 - y_1)^2}},\ x_4(0) = x_{4_0} \tag{15}$$

$$\frac{dy_4}{dt} = \frac{y_1 - y_4}{\sqrt{(x_4 - x_1)^2 + (y_4 - y_1)^2}},\ y_4(0) = y_{4_0},\quad 0 \le t \le t_f \tag{16}$$

Will need to set up the two additional equations for the Euler integration scheme. Figure 1 illustrates the process of Cyclic Pursuit

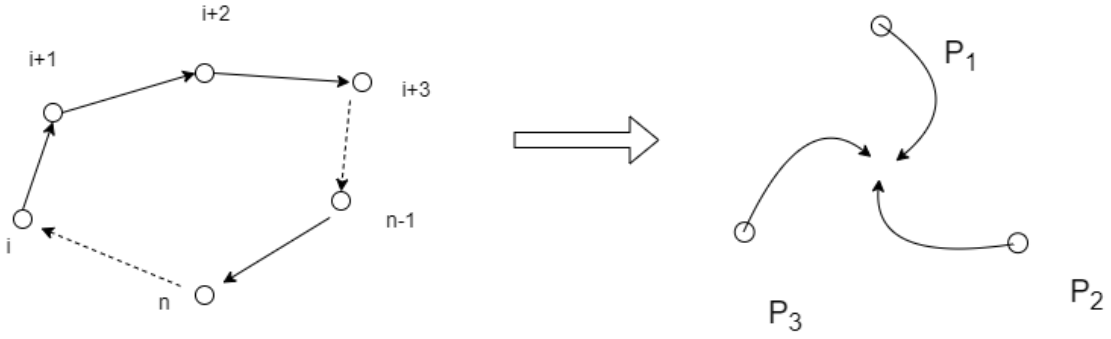


Figure 1: Cyclic Pursuit

### 2.1.4 Evader

We now include an Evader.

The Evader's speed is $\mu$, the Evader's instantaneous position is $(x, y)$ and his control is his instantaneous heading angle $\phi$, measured with respect from the North.

Thus, we now include two more dynamics equations:

$$\frac{dx}{dt} = \mu \sin\phi,\ x(0) = x_0 \tag{17}$$

$$\frac{dy}{dt} = \mu \cos\phi,\ y(0) = y_0,\ 0 \leq t \leq t_f \tag{18}$$

so when using the Euler integration scheme we have

$$x(t + dt) = x(t) + \mu \sin\phi(t),\ x(0) = x_0 \tag{19}$$

$$y(t + dt) = y(t) + \mu \cos\phi(t),\ x(0) = x_0 \tag{20}$$

The Evader's control time history $\phi(t),\ 0 \leq t \leq t_f$ has yet to be specified. Also the three Pursuers' and the Evader's initial position $(x_0, y_0)$ must be specified.

We endow the Pursuers with capture circles of radius $l$, say $l = 0.1$. Thus, the capture time $t_f$ is determined by the condition

$$
\begin{aligned}
&min\ (\ (x-x_1)^2+(y-y_1)^2,\ (x-x_2)^2 \\
&+(y-y_2)^2\ (x-x_3)^2+(y-y_3)^2\ )\ |_{t_f}= l^2
\end{aligned}
\tag{21}
$$

We will assume the Evader's speed $0 \leq \mu \leq 1$.

The time-to-capture $t_f$ is determined by equation (21). Thus, keep a record of the variables $a(t) \equiv (x(t)-x_1(t))^2+(y(t)-y_1(t))^2$, $b(t) \equiv (x(t)-x_2(t))^2+(y(t)-y_2(t))^2$, $c(t) \equiv (x(t)-x_3(t))^2+(y(t)-y_3(t))^2$, $0 \leq t$. At each point in time $0 \leq t$ calculate $d(t) \equiv min\ (\ a(t), b(t), c(t)\ )$ and $t_f$ is when $d(t_f) = l^2$.

When does capture occur? Capture happens whenever at least one of the distances between a pursuer and the evader is equal to or less than that evaders' capture range. In mathematical notation, capture happens if $\frac{\sqrt{dt}}{l} \leq 1$ The determination whether capture happens is a function of $\mu, l, r$.

The Evader's strategy is a *state feedback* strategy, not open-loop like in Scenario 1. He (Evader) now tries to escape by breaking through between $P_1$ and $P_3$ but he correctly realizes that the situation is dynamic: Now his control entails state feedback – the Evader heads toward the instantaneous mid-point $M = (x_M, y_M)$ of the segment $\overline{P_1P_3}$. His instantaneous heading is calculated as follows. Let

$$
x_M = \frac{1}{2}(x_1+x_3),\ y_M = \frac{1}{2}(y_1+y_3)
$$

whereupon

$$
\sin\phi(x,y,x_1,y_1,x_3,y_3) = \frac{x_M-x}{\sqrt{(x_M-x)^2+(y_M-y)^2}} \tag{22}
$$

$$
\cos\phi(x,y,x_1,y_1,x_3,y_3) = \frac{y_M-y}{\sqrt{(x_M-x)^2+(y_M-y)^2}} \tag{23}
$$

and eqs. (20) and (21) must be inserted into eqs. (15)-(18), so

$$\frac{dx}{dt} = \mu \frac{x_M - x}{\sqrt{(x_M - x)^2 + (y_M - y)^2}},\ x(0) = x_0 \tag{24}$$

$$\frac{dy}{dt} = \mu \frac{y_M - y}{\sqrt{(x_M - x)^2 + (y_M - y)^2}},\ y(0) = y_0,\ 0 \leq t \leq t_f \tag{25}$$

so, when using the Euler integration scheme we have

$$x(t + dt) = x(t) + \mu \frac{x_M - x}{\sqrt{(x_M - x)^2 + (y_M - y)^2}} \cdot dt,\ x(0) = x_0 \tag{26}$$

$$y(t + dt) = y(t) + \mu \frac{y_M - y}{\sqrt{(x_M - x)^2 + (y_M - y)^2}} \cdot dt,\ x(0) = x_0 \tag{27}$$

where

$$x_M = \frac{1}{2}(x_1 + x_3),\ y_M = \frac{1}{2}(y_1 + y_3)$$

Note: The dynamics are now nonlinear.

Breakout: If the Evader is fast enough ($\mu >> 0$) and the Pursuers' $P_1$ and $P_3$ capture range is short ($0 < l << 1$), E might reach the midpoint M between the Pursuers $P_1$ an$P_2$, say at time $t_b$ and both $a(t_b) > l^2$ and $c(t_b) > l^2$ – in other words, E is not captured. E should now change his strategy and start running away from point M. Thus, in the dynamic's equations (24)-(27) the sign in front of $\mu$ changes to -.

When E seats on the fence, so to speak, this creates an implementation problem when the above-mentioned required sign change is done "out of sync.". This results in the undesirable phenomenon of chatter, whereby E heads toward the aim point M, then away from M, and back toward M.... This is a numeric issue. One way to address it is as follows.

The equation of the straight line which connects the points $P_1$ and $P_3$ is

$$y = \frac{1}{x_1 - x_3}[(y_1 - y_3)x + y_3x_1 - y_1x_3]$$

The x-coordinate of the instantaneous position of E is x. When the expression

$$z(x) \equiv \frac{1}{x_1 - x_3}[(y_1 - y_3)x + y_3x_1 - y_1x_3] > 0 \tag{28}$$

E is still inside the triangle, so the sign in front of $\mu$ in eqs. (26) and (27) is still +. Initially, at time $t = 0$, E is at the center of the equilateral triangle, so E is inside the triangle and the expression (28) is positive. There might however come a time $t_b$ when having exercised equations (26) and (27) and just calculated $x(t_b + dt)$ and $y(t_b + dt)$, while $a(t_b) > l^2$ and $c(t_b) > l^2$, the expression (28) has just changed sign to -. Before continuing with the integration, that is, exercising eqs. (26) and (27), it is time to change the sign in front of $\mu$ to minus.

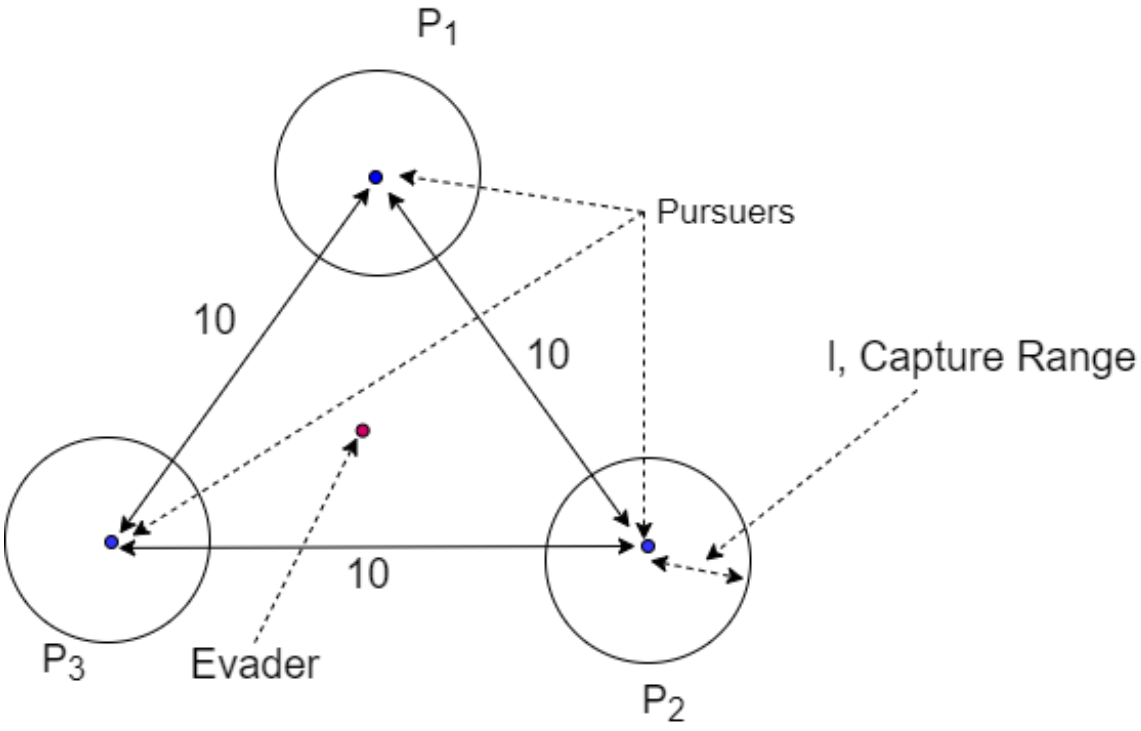


Figure 2: Three equidistant pursuers and one evader

# III. Methodology

## 3.1 Regions of Capturability and escape

### 3.1.1 Design

We now consider the case where initially the evader is not at the center of the equilateral triangle and we will numerically (by simulation) determine when the evader is able to escape from the encirclement enforced by cyclic pursuit. This will very much depend on parameter $\mu$ and $l$; we will work to map out the initial state's region near the center of the equilateral triangle where cyclic pursuit brings capture. Thus, we will place the evader on the circumference of a circle of radius r =0.1, 0.2, 0.3, ...centered at the center of an equilateral triangle.

We will consider the case where initially the pursuers' configuration is not an equilateral triangle. The case of an Isosceles triangle scenario is an intriguing type. During cyclic pursuit, two pursuers come together and then they both coalesce with third pursuers. See Fig 3.

We'll also change the parameters in the simulation until the evader manages to escape. Note, for capturability the parameters need to be: small $\mu$ and/or big $l$ .

We'll let the evader dynamically choose the breakout gap between two of the tree pursuers. However, it is tempting to run toward the midpoint M of the larger gap, say the gap between $P_1$ and $P_3$ but the evader might be closer to the smaller group, say $P_1$ and $P_2$, so it is not clear what the optimal strategy of the evader should be.

#### 3.1.1.1 Strategy

The evader considers the "escape cones": There are three escape cones, because $E$ can try to pass between $P_1$ and $P_2$, between $P_2$ and $P_3$ and between $P_3$ and $P_1$. The three escape cones have a common vertex, E -see figure 4. Thus, there are three aim

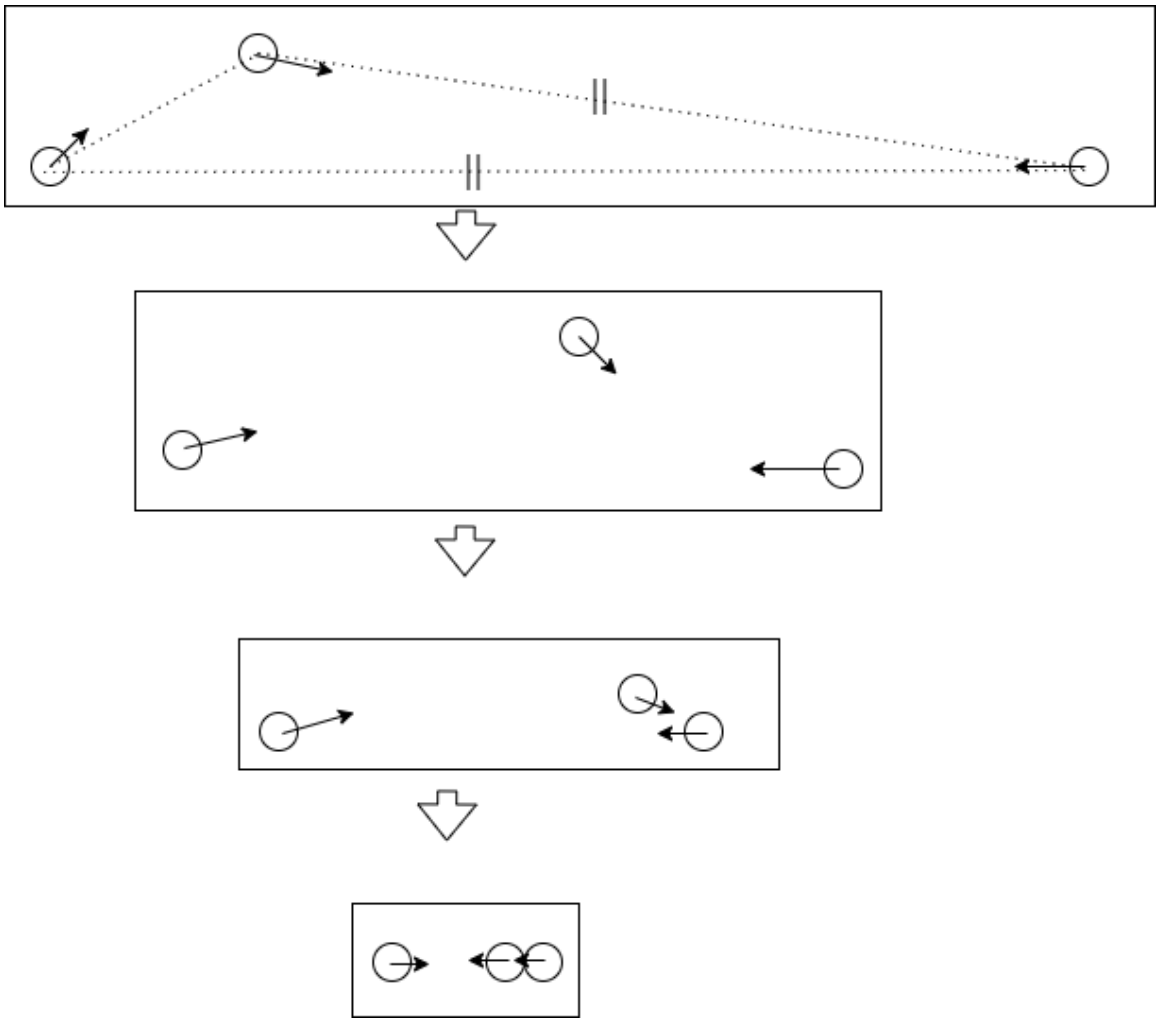

Figure 3: The pursuers coalesce

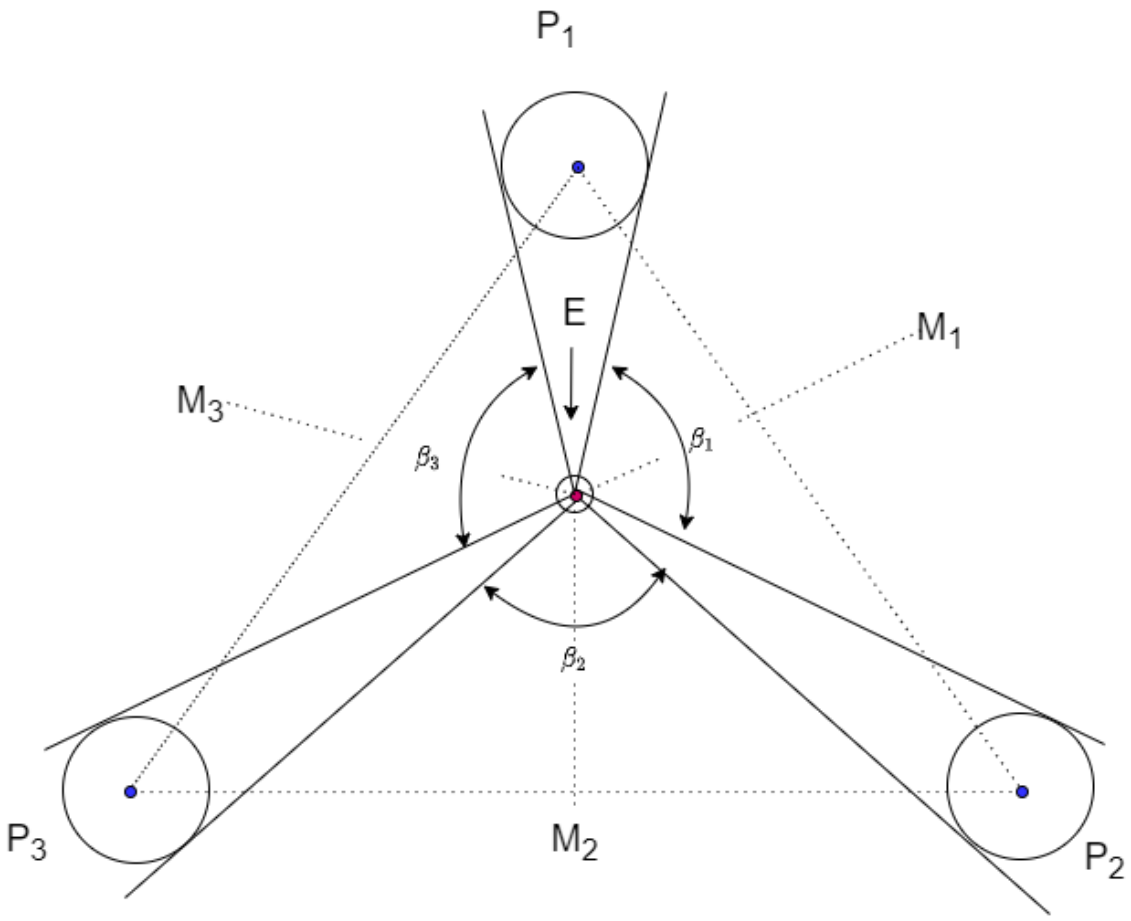


Figure 4: Diagram of escape cones for evader, E

points M, one in each escape cone -point $M_1$ in the escape cone defined by $E$, $P_1$ and $P_2$, point $M_2$ in the escape cone defined by $E$, $P_2$ and $P_3$ and point $M_3$ in the escape cone defined by $E$, $P_3$ and $P_1$. The evader calculates the angle $\beta_i, i = 1, 2, 3$, of the three cones: we use the "Law of the cosines." The escape cone is the one with the biggest angle. Note: $dist(E, P_1) \equiv \sqrt{(x - x_1)^2 + (y - y_1)^2}$

$dist(E, P_2) \equiv \sqrt{(x - x_2)^2 + (y - y_2)^2}$

$dist(E, P_3) \equiv \sqrt{(x - x_3)^2 + (y - y_3)^2}$

$dist(P_1, P_2) \equiv \sqrt{(x_2 - x_1)^2 + (y_2 - y_1)^2}$

$dist(P_1, P_3) \equiv \sqrt{(x_3 - x_1)^2 + (y_3 - y_1)^2}$

$dist(P_3, P_2) \equiv \sqrt{(x_2 - x_3)^2 + (y_2 - y_3)^2}$

We calculate

$\beta_1 = \arccos(\frac{dist^2(E,P_1)+dist^2(E,P_2)-dist^2(P_1,P_2)}{2dist^2(E,P_1)dist^2(E,P_2)})$

$\beta_2 = \arccos(\frac{dist^2(E,P_2)+dist^2(E,P_3)-dist^2(P_2,P_3)}{2dist^2(E,P_2)dist^2(E,P_3)})$

$\beta_3 = \arccos(\frac{dist^2(E,P_1)+dist^2(E,P_3)-dist^2(P_1,P_3)}{2dist^2(E,P_1)dist^2(E,P_3)})$

Let

$$i^* = \arg max_{1 \leq i \leq 3} \beta_i \tag{29}$$

E heads towards the aim point $M_{i^*}$, see Figure 4.

It is important to point out that when E is initially at the center of an equilateral triangle (see Fig 2), E is isochronously captured by the three pursuers. This is because the pursuers are equidistant, and they are also traveling at the same speed. This is not the case when the pursuers are not equidistant or when the evader is not at the center- such as when $r > 0$. Relevant experiments and results can be found in the Results section.

### 3.2 Temporal evolution of the distance between two pursuers during cyclic pursuit

Consider the $\triangle P_1P_2P_3$ formed by the three pursuers in cyclic pursuit where $P_1$ goes after $P_2$, $P_2$ goes after $P_3$ and $P_3$ "closes the loop" by going after $P_1$. We shall first assume that initially the pursuers' formation is an acute $\triangle P_1P_2P_3$ whose sides are $r_1,\ r_2,\ r_3$. The state of the pursuers' formation is specified by $(r_1,\ r_2,\ r_3)$.

We shall use the following non-dimensional variables: $r \to \frac{r}{l}$, $l = 1$, $t \to \frac{v_P}{l}t$ and the speed ratio parameter $\mu = \frac{v_E}{v_P}$, whereupon the dynamics are

$$\dot{r_1} = -1 - \cos P_3,\ r_1(0) = r_{1_0}$$

$$\dot{r_2} = -1 - \cos P_1,\ r_1(0) = r_{2_0}$$

$$\dot{r_3} = -1 - \cos P_2,\ r_1(0) = r_{3_0}$$

Concerning the initial state, we shall assume, without loss of generality

$$\text{Assumption:} \quad r_{1_0} > r_{2_0} > r_{3_0} > 2$$

The lengths of the triangle's three sides is always monotonically decreasing, irrespective of whether $\triangle P_1P_2P_3$ is acute or obtuse.

Because in a triangle the angle opposite a longer side is larger than the angle opposite a shorter side, the following holds: In view of our assumption, initially, for sufficiently small $t$, the angles $\frac{\pi}{2} > P_1 > P_2 > P_3$ and therefore $\mid \dot{r_1}(t) \mid > \mid \dot{r_2}(t) \mid$ and $\mid \dot{r_1}(t) \mid > \mid \dot{r_3}(t) \mid > \mid \dot{r_2}(t) \mid$. Hence, after some time, the curves $r_1(t)$ and $r_2(t)$ will meet, so the lengths of the $r_1$ and $r_2$ sides will become equal. Furthermore, either (i) The curves $r_1(t)$ and $r_2(t)$ will intersect before the curve $r_3(t)$ hits bottom, that is, the length of the side $r_3$ shrinks to zero – for if this were not the case, there would be a

time $t$, where $r_1(t) - r_2(t) > r_3(t)$ and this would violate a triangle inequality, or, (ii) The curves $r_1(t)$ and $r_2(t)$ will intersect at the same time the curve $r_3(t)$ hits bottom, that is, $r_3 = 0$ and $r_1 = r_2$ – in this case the above mentioned triangle inequality is not violated. Hence, there will be a time $t$ where either (i) The pursuers' formation, $\triangle P_1P_2P_3$, becomes isosceles, or, (ii) The pursuers $P_1$ and $P_3$ coalesce, whereupon the triangle will devolve into a shrinking segment until the third pursuer $P_3$ comes together in head on fashion with the ($P_1$,$P_2$) pursuer cluster and the action will be akin to a train wreck. In case (ii) the three pursuers coalesce and "the game is over", but they did not come together isochronously.

In case (i) the $\triangle P_1P_2P_3$ will momentarily be isosceles with $r_3 < r_1 = r_2$, so the angles $P_1 = P_2 > P_3$, and its vertex angle $P_3 < \frac{\pi}{3}$. Hence at the point in time $\mid \dot{r_1}(t) \mid > \mid \dot{r_2}(t) \mid = \mid \dot{r_3}(t) \mid$, so the length of the side $r_1$ decreases faster than the length of the side $r_2$ and $\triangle P_1P_2P_3$ will be isosceles during a fleeting time only – see Fig. 15. At some point in time further down the line the curves $r_1(t)$ and $r_3(t)$ in Fig. 15 will meet and a new, smaller, isosceles $\triangle P_1P_2P_3$ will be formed – the curve $r_3(t)$ cannot avoid meeting the curve $r_1(t)$ by first reaching the t-axis so $r_3(t) = 0$ while $r_2(t) > r_1(t)$ – see Fig. 15 . Thus, the new isosceles $\triangle P_1P_2P_3$ has the sides $r_1 = r_3 < r_2$, the angles $P_1 = P_3 < P_2$, and its vertex angle $P_2 > \frac{\pi}{3}$. The angles $P_2 > P_1 = P_3$ and therefore momentarily $\mid \dot{r_1}(t) \mid = \mid \dot{r_2}(t) \mid > \mid \dot{r_3}(t) \mid$ and therefore, down the road – see Fig. 15 – the curves $r_2(t)$ and $r_3(t)$ will meet so the lengths of the $r_2$ and $r_3$ sides will become equal, $r_2(t) = r_3(t) > r_1(t)$, the angles $P_2 = P_3 > P_1$ a new isosceles triangle will be formed, this time its vertex being $P_1$, and the angle $P_1 < \frac{\pi}{3}$. So far, while the formation $\triangle P_1P_2P_3$ has been shrinking, one cycled through a sequence of three isosceles triangle whose respective vertices in turn were $P_3$, $P_2$ and $P_1$. In the last instance, where the angles $P_2 = P_3 > P_1$, $\mid \dot{r}_1 \mid = \mid \dot{r}_3 \mid < \mid \dot{r}_2 \mid$. The temporal

evolution of the lengths of the sides of the triangle is shown in Fig. 16: The curves $r_1(t)$ and $r_2(t)$ will meet and an isosceles triangle whose sides $r_1(t) = r_2(t) < r_3(t)$ and its vertex is $P_3$ ( $> \frac{\pi}{3}$ ) will be formed. We have come around full circle.

If the $\triangle P_1P_2P_3$ is initially obtuse, the above analysis still applies: In view of our Assumption, initially, for sufficiently small $t$, the angles $P_1 > P_2 > P_3$, but now $P_1 > \frac{\pi}{2}$. Therefore $\mid \dot{r_2}(t) \mid < 1$, whereas, as before, $\mid \dot{r_1}(t) \mid > \mid \dot{r_3}(t) \mid > 1$. Thus, as before, $\mid \dot{r_1}(t) \mid > \mid \dot{r_3}(t) \mid > \mid \dot{r_2}(t) \mid$. Hence, the action is as in Fig. 16 and after some time – see the temporal evolution of the lengths of the sides in Fig. 16 – the curves $r_1(t)$ and $r_2(t)$ will meet, so the lengths of the $r_1$ and $r_2$ sides will become equal, the $\triangle P_1P_2P_3$ will momentarily be isosceles, now, with $P_1 < \frac{\pi}{2}$, and, as before, this cycle will repeat.

One must also consider the possibility of a "flat" triangle – think of a triangle with e.g., $P_1 = 88$ deg, $P_2 = 86$ deg, $P_3 = 6$ deg. Thus, consider a newly formed "flat" isosceles triangle, with $r_1(0) = r_2(0) = r$ and $r_3(0) = \epsilon \cdot r,\ \epsilon << 1$. The non linear dynamics of the pursuers' formation are

$$\begin{aligned} \dot{r_1} &= -1 - \frac{r_1^2 + r_2^2 - r_3^2}{2r_1r_2},\ r_1(0) = r_{1_0} \\ \dot{r_2} &= -1 - \frac{r_2^2 + r_3^2 - r_1^2}{2r_2r_3},\ r_2(0) = r_{2_0} \\ \dot{r_3} &= -1 - \frac{r_1^2 + r_3^2 - r_2^2}{2r_1r_3},\ r_3(0) = r_{3_0} \end{aligned} \tag{30}$$

and we calculate

$$\dot{r_1}(0) \approx -2 + \frac{1}{2}\epsilon^2,\quad \dot{r_2}(0) \approx -1 - \frac{1}{2}\epsilon,\quad \dot{r_3}(0) \approx -1 - \frac{1}{2}\epsilon$$

In non-dimensional time $\frac{1}{2}\epsilon$ the triangle's sides will be $r_1(\frac{1}{2}\epsilon) \approx r - \epsilon$, $r_2(\frac{1}{2}\epsilon) \approx r - \frac{1}{2}\epsilon$,

$r_3(\frac{1}{2}\epsilon) \approx \frac{1}{2}\epsilon$, so the triangle will be further flattened, the three pursuers converging to a configuration where they are almost collinear, arranged like ducks in a row, $P_1,\ P_2,\ P_3$, with $r_2 = r_1 + r_3$, $0 < r_3 << 1$, and the closing speeds being $\dot{r}_1 = \dot{r}_2 = -2,\ \dot{r}_3 = 0$, as expected. The pursuers $P_2$ and $P_3$ then come together forming a cluster of two pursuers in a head on encounter with the third, close by, pursuer $P_1$. The three pursuers end up coming together.

Finally, note that the dynamical system (30) *globally* converges in $finite$ time to its unique rest point/equilibrium $r_1 = r_2 = r_3 = 0$.

The following holds:

#### 3.2.0.1 Proposition

A triangular formation with three pursuers in cyclic pursuit with ranges $r_1 > r_2 > r_3$ will evolve so that at some point in time it forms an isosceles triangle, albeit for a fleeting moment. Further down the road a sequence of ever smaller isosceles triangles is momentarily formed, their vertices forming a periodic sequence $P_3, P_2, P_1, P_3, P_2, P_1, P_3$...., with $P_3 < \frac{\pi}{3}, P_2 > \frac{\pi}{3}, P_1 < \frac{\pi}{3}, P_3 > \frac{\pi}{3}$... It is also possible that the three pursuers momentarily converge to a configuration where they are almost collinear, arranged like ducks in a row, $P_1, P_2, P_3$, with $r_2 = r_1 + r_3, 0 < r3 \ll 1$, the closing speeds being $\dot{r}_1 = \dot{r}_2 = -2, \dot{r}_3 = 0$, as expected. The pursuers $P_2$ and $P_3$ then come together forming a cluster of two pursuers in a head on encounter with the close by pursuer $P_1$, whereupon the three pursuers end up coming together. Irrespective of the initial configuration, the three pursuers come together in finite time.

### 3.2.1 Design and Analysis

Figures 12-31 were generated as results of the simulation. Equation (33) was used for the simulation. The plots, in each case, show the initial lengths of the triangle as its outermost triangle. The plots also show the triangle size and position as it changes with respect to time. We see that for equilateral triangles, which are pursuers that are equidistant from each other, their lengths ($r_1$ , $r_2$ and $r_3$ ) decrease at the same rate all the way to zero. For the acute and obtuse triangles, the pursuers come together in two stages. First two of the three pursuers coalesce then both pursuers join the third pursuer head on. Let's consider the pursuer formation to be $\triangle ABC$ with pursuer $P_1$ at vertex A of the triangle, pursuer $P_2$ at vertex B of the triangle and pursuer $P_3$ at vertex C of the triangle -see figure 5. Our simulation will study the temporal evolution of the sides of the triangles overtime. Through this simulation we should be able to obtain the trajectories of the three pursuers and show how it behaves over a period, $t$, where $0 <\leq t \leq t_f$. The time $t_f$ is when the length of one of the sides of the triangle shrinks to $\epsilon$, $0 < \epsilon \ll 1$. The triangle formed at the very onset of the simulation should gradually shrink as time passes. An $\epsilon$ value of 0.09 was used during this experiment. To get the simulation going, first calculate $r_1$, $r_2$ and $r_3$

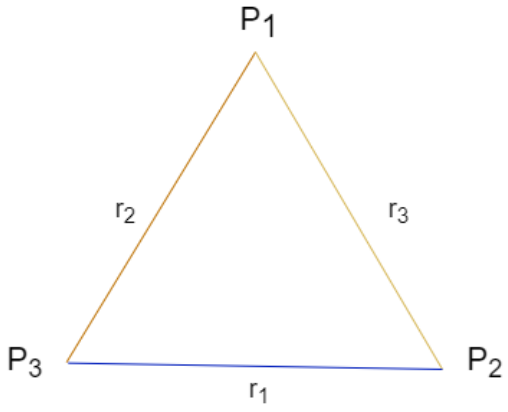


Figure 5: Pursuers triangle

$$
\begin{aligned}
r_1 &= \sqrt{(x_3 - x_2)^2 + (y_3 - y_2)^2}, \\
r_2 &= \sqrt{(x_1 - x_3)^2 + (y_1 - y_3)^2}, \\
r_3 &= \sqrt{(x_2 - x_1)^2 + (y_2 - y_1)^2}
\end{aligned}
\tag{31}
$$

and the angles in the triangle

$$
\begin{aligned}
\cos A &= \frac{{r_2}^2 + {r_3}^2 - {r_1}^2}{2 r_2 r_3}, \\
\cos B &= \frac{{r_1}^2 + {r_3}^2 - {r_2}^2}{2 r_1 r_3}, \\
\cos C &= \frac{{r_1}^2 + {r_2}^2 - {r_3}^2}{2 r_1 r_2}
\end{aligned}
\tag{32}
$$

The dynamics are

$$
\begin{aligned}
\dot{x}_1 &= \frac{x_2 - x_1}{r_3}, x_1(0) = x_{1_0} \\
\dot{y}_1 &= \frac{y_2 - y_1}{r_3}, y_1(0) = y_{1_0} \\
\dot{x}_2 &= \frac{x_3 - x_2}{r_1}, x_2(0) = x_{2_0} \\
\dot{y}_2 &= \frac{y_3 - y_2}{r_1}, y_2(0) = y_{2_0} \\
\dot{x}_3 &= \frac{x_1 - x_3}{r_2}, x_3(0) = x_{3_0} \\
\dot{y}_3 &= \frac{y_1 - y_3}{r_2}, y_3(0) = y_{3_0}
\end{aligned}
\tag{33}
$$

## 3.3 Evolution of Formation

### 3.3.1 Shrinking n-gon

### 3.3.2 Design

Using equations 2-16, simulations was performed on several polygon shaped pursuer formations to see how their formation evolved over time. The prepostion described below was validated in the Results chapter. Experiments using MATLAB were performed on trapezoid, rectangular, square formation to study the evolution of the formation. Pursuers were placed at each vertex of the formation in simulation and their trajectory was plotted over time. The result and analysis of the findings are shown in the Results chapter.

#### 3.3.2.1 Preposition

In general, when the pursuer's formation is a n-gon, the following scenario will occur: Symmetry tends to be preserved – an equilateral triangle will shrink to a continum of smaller equilateral triangles and eventually into a point located at the center of the original triangle. The same happens to a square, which will shrink into smaller and smaller squares until they collapse into a point located at the center of the original square, as displayed in figure 6. A rectangle will shrink into a continuum of parallelograms, which will eventually shrink into a straight line segment, which down the road collapses into a point located at the midpoint of the segment and which is at the center of the original rectangle. Only an irregular n-gon shrinks after some time into a polygon with n-1 sides, and further down the road into a polygon with n-2 sides... , and finally into a segment followed by the midpoint of the segment.

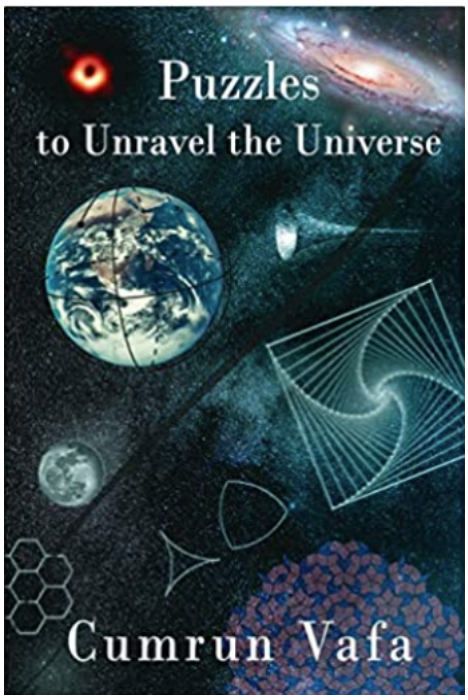


Figure 6: Cyclic Pursuit and the Universe

### 3.4 Capturability

We bring back the evader.

Consider an equilateral pursuer formation. The capture range of the pursuers is $0 < l < \frac{r_0}{2}$. The symmetric case where initially the encircled evader is at the center $O = (0, \frac{1}{2\sqrt{3}} r_0)$ of the equilateral $\triangle P_1 P_2 P_3$ is considered. To fix ideas, consider the case where at time $t = 0$ the pursuers' positions are $P_1 = (0, \sqrt{3})$, $P_2 = (-1, 0)$, $P_3 = (1, 0)$. The initial distance between two pursuers/the length of the side of $\triangle P_1 P_2 P_3$ is $r_0 = 2$ and its center $O = (0, \frac{1}{\sqrt{3}})$.

The kinematics of the pursuers' formation is predictable. The ever shrinking equilateral $\triangle P_1 P_2 P_3$ is rotating about its stationary center $O$. The equilateral's triangle side length is decreasing at the rate $1 + \cos(\frac{\pi}{3}) = \frac{3}{2}$. Hence, at time $t$ the length of

the equilateral's triangle side is $r(t) = r_0 - \frac{3}{2}t = 2 - \frac{3}{2}t$; off the bat we conclude that at time $t_f = \frac{2}{3}r_0 = \frac{4}{3}$ it's all over; in fact, the impenetrable encirclement of the evader is completed at time

$$t_c = \frac{2}{3}(r_0 - 2l)$$

when the capture disks of the pursuers first come into contact; if, for example, $r_0 = 2$,

$$t_c = \frac{4}{3}(1 - l)$$

If for some reason at time $t_c$ the evader is still inside the equilateral $\triangle P_1P_2P_3$, he will be captured irrespective of what his speed $0 \leq \mu$ is. Now, at time $t_c$, an evader which started out at the center $O$ of the equilateral pursuers' formation $\triangle P_1P_2P_3$ will irrevocably be inside the equilateral $\triangle P_1P_2P_3$ if

$$\mu t_c \leq \frac{1}{\sqrt{3}}[\frac{1}{2}(r_0 - \frac{3}{2}t_c)] = \frac{1}{2\sqrt{3}}(r_0 - \frac{3}{2}t_c)$$

that is,

$$t_c \leq \frac{2}{\sqrt{3}(4\mu + \sqrt{3})}r_0 \ ,$$

so as far as the problem parameters $\mu$, $r_0$, $l$ are concerned, the condition is

$$\frac{2}{3}(r_0 - 2l) \leq \frac{2}{\sqrt{3}(4\mu + \sqrt{3})}r_0$$

We conclude:

• If initially E is located at the center $O$ of the triangle and his speed

$$\mu \leq \frac{\sqrt{3}}{2}\frac{l}{r_0 - 2l} \tag{34}$$

in no way can he exit the encirclement triangle before it closes in on him and his capture is a given. In this case, cyclic pursuit is a capture strategy. For example, if $r_0 = 2$, $l = \frac{1}{2}$ and the evader's speed $\mu \leq \frac{\sqrt{3}}{4} \approx 0.433$, there's no way out.

At time $0 \leq t \leq t_f$ the distance from the center $O$ to a vertex of the triangle, is $\overline{OP_i} = \frac{2}{3}r(t)\sin(\frac{\pi}{3}) = \frac{1}{\sqrt{3}}r(t) = \frac{1}{\sqrt{3}}(r_0 - \frac{3}{2}t) = \frac{1}{\sqrt{3}}(2 - \frac{3}{2}t)$, $i = 1, 2, 3$. The component of the $P_i$ pursuer's velocity normal to the radial $\overline{OP_i}$ is $\cos(\frac{\pi}{3}) = \frac{1}{2}$. Hence, at time $t$ the rotation rate $\omega$ of the pursuers' formation/of $\triangle P_1P_2P_3$ is $\omega = \frac{\frac{1}{2}}{\overline{OP_i}}$, so

$$\omega(t) = \frac{\sqrt{3}}{2r_0 - 3t}\ ,\ 0 \leq t < t_f = \frac{2}{3}r_0 \tag{35}$$

If for example $r_0 = 2$,

$$\omega(t) = \frac{\sqrt{3}}{4 - 3t}\ ,\ 0 \leq t < t_f = \frac{4}{3}$$

The formation's rotation rate increases over time and $lim_{t \to t_f}\omega(t) = \infty$.

At time $0 < t < t_f$, $\triangle P_1P_2P_3$ is rotated and its "heading" measured from the positive y-axis

$$\begin{aligned}
\theta(t) &= \int_0^t \omega(t)dt \\
&= \int_0^t \frac{\sqrt{3}}{2r_0 - 3t}dt \\
&= \frac{1}{\sqrt{3}}\ln(\frac{2r_0}{2r_0 - 3t})\ ,\ \ 0 \leq t < t_f\ (\ = \frac{2}{3}r_0\ )
\end{aligned}$$

In fact, once $t = t_c$ ( $= \frac{2}{3}(r_0 - 2l) < t_f = \frac{2}{3}r_0$ ), if the evader is still inside $\triangle P_1P_2P_3$, it's game over. Thus, given $r_0$ and $l$,

$$\theta(t) = \frac{1}{\sqrt{3}} \ln(\frac{2r_0}{2r_0 - 3t}) \ , \quad 0 \leq t < t_c = \frac{2}{3}(r_0 - 2l) \ , \tag{36}$$

so the triangular formation's "maximal" rotation angle

$$\begin{aligned} \theta_c &\equiv \theta(t_c) \\ &= \frac{1}{\sqrt{3}} \ln(\frac{r_0}{2l}) \end{aligned}$$

If for example $r_0 = 2$ and $l = \frac{1}{2}$, $t_c = \frac{2}{3}$ and the triangular formation's "maximal" rotation angle $\theta_c = \frac{1}{\sqrt{3}} \ln(2) = 22.929°$. If at this time ($t_c$) the evader is still inside $\triangle P_1P_2P_3$, his capture is a foregone conclusion.

The rotating gap between two pursuers, which initially was $r_0 - 2l$, decreases at the constant rate $\frac{3}{2}$ and two pursuers' capture disks will come in contact at time $t_c = \frac{2}{3}(r_0 - 2l)$, whereupon the opening between the pursuers closes and the pursuer's formation becomes impenetrable. The escaping evader, who might be well aware of the clockwork kinematics of the pursuers' formation, will try to pass through the opening between two pursuers: Aware of the pursuers' formation kinematics, the evader will head straight toward the *anticipated* opening between two pursuers. To escape the encirclement in the shortest possible time starting out from the center $O$ of $\triangle P_1P_2P_3$, the evader will head straight toward the center $M$ of the *anticipated* opening between two pursuers because this is the shortest distance to a side of $\triangle P_1P_2P_3$. Reaching at time $t$ a side of $\triangle P_1(t)P_2(t)P_3(t)$ not at its center point means that the side of a bigger equilateral $\triangle P_1(t')P_2(t')P_3(t')$ could have been reached by heading toward the midpoint of one of its sides. And since the triangles in the family of

triangles $\triangle P_1(t)P_2(t)P_3(t)$ are nested – because the pursuers employ pure pursuit – and the triangles are shrinking, this implies $t' < t$. In other words, the evader could have escaped earlier. Hence, to escape the encirclement in minimum time the evader will head toward the center $M$ of the *anticipated* opening between two pursuers.

When the pursuers employ cyclic pursuit, the evader is able to break out of the encirclement/$\triangle P_1P_2(t')P_3(t')$ if and only if he can make it to midway between two pursuers before the window of opportunity literally closes at time $t_c$ and his encirclement by the capture disk - endowed pursuers becomes impenetrable. Now, the reachable set at time $t$ of the holonomic evader is a circular disk of radius $\mu t$ centered at $O$. The evader cannot make it through an opening between two pursuers and consequently will come in contact with, and will be absorbed by, a pursuer's capture disk if there does not exist a $0 < t < t_c$ s.t. $\mu t > \overline{OM}(t)$, where $M$ is the midpoint of the opening between two pursuers and, as such, is also the midpoint of a side of the triangle at time $t$. The segment $\overline{OM}(t) = \frac{1}{2\sqrt{3}}r(t)$. Thus, even a well informed evader starting out from the center $O$ of the equilateral triangle will inevitably come in contact with a pursuer's capture disk and will be captured if

$$\mu t \leq \frac{1}{2\sqrt{3}}(r_0 - \frac{3}{2}t) \ , \ \forall \ 0 < t \leq t_c$$

that is, if

$$(\mu + \frac{\sqrt{3}}{4})t \leq \frac{1}{2\sqrt{3}}r_0 \ , \ \forall \ 0 < t \leq t_c \ (= \frac{2}{3}(r_0 - 2l))$$

This will be the case if

$$(\mu + \frac{\sqrt{3}}{4})\frac{2}{3}(r_0 - 2l) \leq \frac{1}{2\sqrt{3}}r_0$$

If condition (34) holds, this is indeed the case: Even a well informed evader starting out from the center $O$ of the equilateral triangle will be captured. An evader which initially is at the center of an equilateral pursuer formation whose size is $r_0$ and the pursuers are endowed with capture disks of radius $l$, but which is informed about the pursuers' cyclic pursuit strategy, can escape from encirclement by cyclic pursuit, if and only if his speed

$$\mu > \frac{\sqrt{3}}{2}\frac{l}{r_0 - 2l} \tag{37}$$

An alternative, somewhat superfluous, derivation of eq. (37) proceeds as follows. escape by passing between two pursuers is possible if and only if $\exists\ t > 0$ s.t. $\overline{OM}(t) \leq \mu t$ and $r_0 - \frac{3}{2}t - 2l > 0$. Thus, a solution $t$ to the following two inequalities must exist.

$$\frac{1}{2\sqrt{3}}(r_0 - \frac{3}{2}t) \leq \mu t$$
$$r_0 - \frac{3}{2}t - 2l > 0$$

Hence, $t$ must satisfy the inequalities

$$\frac{r_0}{2\sqrt{3}(\mu + \frac{\sqrt{3}}{4})} < t < \frac{2}{3}(r_0 - 2l)$$

These inequalities can be satisfied if the problem parameters satisfy the requirement

$$\frac{r_0}{2\sqrt{3}(\mu + \frac{\sqrt{3}}{4})} < \frac{2}{3}(r_0 - 2l)$$

which will be the case if the evader's speed

$$\mu > \frac{\sqrt{3}}{2}\frac{l}{r_0 - 2l}$$

Equation (37) has been recovered !

From eq. (34) we conclude that starting out from the center $O$ of a "small" equilateral formation whose size

$$2l < r_0 < (2 + \frac{\sqrt{3}}{2})l \ , \tag{38}$$

a "slow" evader whose speed $\mu \leq 1$, cannot escape from cyclic pursuit – this is so because the R.H.S. of eq. (36) is then bigger than 1. From eq. (37) we conclude that starting out from the center $O$ of a "small" equilateral formation whose size is s.t. condition (38) holds, then in order to be able to escape, even a well informed evader will have to be a "fast" evader, that is, an evader whose speed $\mu > 1$ – this is so because the R.H.S. of eq. (37) is then bigger than 1. If however the formation is big enough, that is,

$$r_0 > 2l + \frac{\sqrt{3}}{2}$$

so that the R.H.S. of eq. (37) is less than 1, then starting out from the center of an equilateral pursuer formation, a well informed "fast" evader, that is, an evader whose speed $\mu > 1$, can escape from cyclic pursuit. Of course, also a well informed "slow" evader, that is, an evader whose speed $\mu < 1$, will be able to escape from cyclic pursuit when the pursuers' formation is "big" enough so that the R.H.S. of eq. (37) is less than 1, provided that condition (37) holds. Note however that if condition

(34) holds, even a "fast" evader is doomed.

In summary, it's all about the problem parameters $r_0$, $l$ and $\mu$, as quantified by eq. (37).

From eq. (37) we deduce that in the case of point capture, where $l = 0$, the requirement is $\mu > 0$, that is, the informed evader's escape is always possible, even if the evader is a snail !

We conclude:

- In the case of cyclic pursuit, the often used/overused in pursuit-evasion differential games "point capture" paradigm makes no sense.

When the pursuers' capture range $0 < l << 1$, escape from cyclic pursuit is a no brainer. The bigger the pursuers' capture range $l$ is, the faster the evader must be for escape from the encirclement to be possible – see eq. (37). If for example the capture range $l = \frac{1}{4}r_0$, need $\mu > \frac{\sqrt{3}}{4}$. And if $\frac{1}{2}r_0 > l > \frac{2}{4+\sqrt{3}}r_0$, the evader must be "fast", that is, need $\mu > \frac{\sqrt{3}}{2}\frac{l}{r_0-2l} > 1$.

Given the problem parameters $r_0$, $l$ and $\mu$, if condition (37) holds, the evader proceeds to plan his escape from cyclic pursuit as follows. Without loss of generality consider the case where the evader attempts to slip through between pursuers $P_1$ and $P_3$. He'll

escape the encirclement by passing between two pursuers at time $t_e$, which is provided by the solution of the equation $\overline{OM}(t_e) = \mu t_e$, that is,

$$\frac{1}{2\sqrt{3}}(r_0 - \frac{3}{2}t_e) = \mu t_e$$

The evader will escape the encirclement at time

$$t_e = \frac{2}{\sqrt{3}} \cdot \frac{r_0}{4\mu + \sqrt{3}} \ , \tag{39}$$

provided $t_e < t_c$, that is

$$\frac{2}{\sqrt{3}} \frac{1}{4\mu + \sqrt{3}} r_0 < \frac{2}{3}(r_0 - 2l)$$

This requires the evader's speed $\mu$ to satisfy condition (37), which is our standing assumption. When the three problem parameters are s.t. condition (37) holds, the well informed evader can break out of the encirclement at time $t_e$ – see eq. (39).

For example, if $r_0 = 2$, the escape time from encirclement is $t_e = \frac{4}{4\sqrt{3}\mu+3}$, provided $\mu > \frac{\sqrt{3}}{4}\frac{l}{1-l}$, and if in addition $l = \frac{1}{2}$, the condition is $\mu > \frac{\sqrt{3}}{4}$; in our example we use $\mu = \frac{\sqrt{3}}{2}$, so escape from encirclement is possible.

At time $t_e$ – see eq. (36) – the triangle will have rotated in a clockwise direction by an angle

$$\theta(t_e) = \frac{1}{\sqrt{3}} \ln(1 + \frac{\sqrt{3}}{4\mu})$$

Let

$$\theta_e \equiv \theta(t_e) = \frac{1}{\sqrt{3}} \ln(1 + \frac{\sqrt{3}}{4\mu})$$

• The angle $\theta_e$ does *not* depend on the initial size $r_0$ of the $\triangle P_1P_2P_3$ formation.

$\theta_e < \theta_c$ ( $= \frac{1}{\sqrt{3}} \ln(\frac{r_0}{2l})$ ) if and only if our standing assumption, eq. (37), holds. And since the parameter $\mu$ satisfies condition (37), our standing assumption, given $r_0$ and $l$ with the proviso that $r_0 > 2l$, the rotation angle at escape time is bounded:

$$0 < \theta_e < \frac{1}{\sqrt{3}} \ln(2\frac{r_0}{l} - 3) \; ( < \theta_c = \frac{1}{\sqrt{3}} \ln(\frac{r_0}{2l}) \; )$$

If, as in our example, $r_0 = 2$, $l = \frac{1}{2}$ and the evader's speed is the critical speed $\mu = \frac{\sqrt{3}}{4}$, then $t_e = t_c$ and the pursuers' formation rotation angle $\theta_e = \theta_c = \frac{1}{\sqrt{3}} \ln(2)$, that is, $\theta_e \approx 22.929^\circ$ – as expected. Although the evader made it to the pursuers' formation perimeter, he'll be captured at time $t_e$ by the pursuer $P_1$. However, in our example the evader's speed $\mu = \frac{\sqrt{3}}{2}$, so the rotation angle $\theta_e = \frac{1}{\sqrt{3}} \ln(\frac{3}{2})$, that is, $\theta_e \approx 13.412^\circ$ ( $< \theta_c = 22.929^\circ$ ).

To escape the encirclement in minimum time the well informed evader will hold the course

$$\begin{aligned} \psi^* &= \theta_e + \frac{\pi}{3} \\ &= \frac{1}{\sqrt{3}} \ln(1 + \frac{\sqrt{3}}{4\mu}) + \frac{\pi}{3} \end{aligned}$$

and pass between $P_1$ and $P_3$ at time $t_e = \frac{2}{\sqrt{3}} \frac{r_0}{4\mu + \sqrt{3}}$. The escape path course ($\psi^*$) does *not* depend on the initial size $r_0$ of the equilateral $\triangle P_1P_2P_3$, however the attendant

escape time $t_e$ is linearly dependent on $r_0$.

For example, when $r_0 = 2$, $t_e = \frac{4}{4\sqrt{3}\mu+3}$.

In light of the above, the optimal escape path of the evader is

$$x_E(t) = \mu t \sin\psi^* \ , \quad y_E(t) = \mu t \cos\psi^* + \frac{1}{2\sqrt{3}} r_0 \ , \ 0 \le t \le t_e$$

that is,

$$\begin{aligned} x_E(t) &= \frac{1}{2}\mu t[\sin(\frac{1}{\sqrt{3}}\ln(1+\frac{\sqrt{3}}{4\mu})) + \sqrt{3}\cos(\frac{1}{\sqrt{3}}\ln(1+\frac{\sqrt{3}}{4\mu}))] \ , \\ y_E(t) &= \frac{1}{2}\mu t[\cos(\frac{1}{\sqrt{3}}\ln(1+\frac{\sqrt{3}}{4\mu})) - \sqrt{3}\sin(\frac{1}{\sqrt{3}}\ln(1+\frac{\sqrt{3}}{4\mu}))] + \frac{1}{2\sqrt{3}} r_0 \ , \\ & 0 \le t \le t_e = \frac{2}{\sqrt{3}} \frac{r_0}{4\mu+\sqrt{3}} \end{aligned} \tag{40}$$

The optimal escape path of the evader does not depend on $r_0$ and $l$, only on his speed $\mu$ – this, provided condition (34) holds.

The analysis is summarized in the following

Theorem 1 An evader which initially is at the center of an equilateral pursuer formation whose size is $r_0$ and the pursuers are endowed with capture disks of radius $l$ will be captured in cyclic pursuit if he is not fast enough, that is, condition (31) holds. An evader which initially is at the center of an equilateral pursuer formation whose size is $r_0$ and the pursuers are endowed with capture radius $l$, but which is informed about the pursuers' cyclic pursuit strategy, can escape from encirclement by cyclic

pursuit, if and only if his speed is s.t. condition (34) holds. Furthermore, to escape the encirclement by cyclic pursuit in minimum time

$$t_e = \frac{2}{\sqrt{3}} \cdot \frac{r_0}{4\mu + \sqrt{3}} \ ,$$

the evader hods the course

$$\psi^* = \frac{1}{\sqrt{3}} \ln(1 + \frac{\sqrt{3}}{4\mu}) + \frac{\pi}{3}$$

Proof If condition (37) does not hold the pursuers' capture disks will come into contact before the evader can reach a side of the shrinking $\triangle P_1P_2P_3$. Capture is then preordained. If condition (37) holds an informed evader is able to escape the encirclement by holding the course $\psi^*$ and cross a side of $\triangle P_1P_2P_3$ by passing through the midpoint $M$ between two pursuers. If the informed evader is not able to pass unscathed in the middle between two pursuers before their capture disks come into contact, he is not able to break out of the encirclement. This is so because aiming at the triangle's midpoint $M$ provides the shortest path to freedom. Hence, condition (37) is a necessary and sufficient condition for an informed evader to be able to escape the encirclement by cyclic pursuit. The strategy of holding the course $\psi^*$ lets the informed evader escape the encirclement by cyclic pursuit in minimum time. This is so because the family of shrinking triangles is nested. The latter is a result of the fact that in cyclic pursuit the pursuers employ pure pursuit. □

• We choose $r_0 = 2$ and $\mu$ and $l$ parameters s.t. condition (37) is satisfied, say, $l = \frac{1}{2}$, $\mu = \frac{\sqrt{3}}{2}$ ($> \frac{\sqrt{3}}{4}$), and also $\mu = \frac{1}{2}$ ($> \frac{\sqrt{3}}{4}$), and perform a simulation/animation (see figure 38, 39 ,41 and 42) where E's straight line escape trajectory will be traced as he escapes the maelstrom of rotating and shrinking triangles which are closing in

on him.

We'll also do the case where condition (37) is not satisfied – the pursuers close ranks before the evader manages to exit the pursuers' encirclement and the evader's capture is preordained (see figure 40). As before, $r_0 = 2$, $l = \frac{1}{2}$, but now $\mu = \frac{1}{4}$ ($< \frac{\sqrt{3}}{4}$).

# IV. Results and Analysis

## 4.1 Regions of Capturability and escape

### 4.1.1 Equidistant Pursuers - Equilateral Triangle

#### 4.1.1.1 Evader at the center at radius, r = 0

With E in the center of the equidistant pursuers (Fig 2), simulations (using MATLAB) were conducted for scenarios with speed, $\mu$ ranging from 0.0 to 2.0 in 0.2 increment and initial capture range, $l$, ranging from 20% (1.15 units) range to 80% (4.612 units) in 20% increments. 100% capture range is defined as the distance from any of the pursuers to the evader at time $dt = 0$ The results are displayed Table 1 and in a 3D plot in Fig 7. Figure 7 reveals clearly that more capture happens as capture range increases. Table 1 shows the value for $t_f$ for the varied values of $\mu$ and $l$ which shows a decrease in $t_f$ as speed increases

Table 1: Table showing result from Evader at the center of the equilateral triangle

| **Evader Speed** | **Pursuer's capture range as fraction of the initial length of the triangle's side** | | | |
|---|---|---|---|---|
| $\mu$ | 20 % | 40 % | 60 % | 80 % |
| 0.000 | 5.400 | 4.080 | 2.720 | 1.400 |
| 0.200 | 4.720 | 3.600 | 2.440 | 1.240 |
| 0.400 | 4.640 | 3.440 | 2.240 | 1.120 |
| 0.600 | Escaped | 3.440 | 2.080 | 1.040 |
| 0.800 | Escaped | 3.400 | 2.000 | 1.000 |
| 1.000 | Escaped | Escaped | 2.000 | 0.920 |
| 1.200 | Escaped | Escaped | 2.000 | 0.880 |
| 1.400 | Escaped | Escaped | 1.960 | 0.840 |
| 1.600 | Escaped | Escaped | 1.960 | 0.800 |
| 1.800 | Escaped | Escaped | Escaped | 0.760 |
| 2.000 | Escaped | Escaped | Escaped | 0.760 |

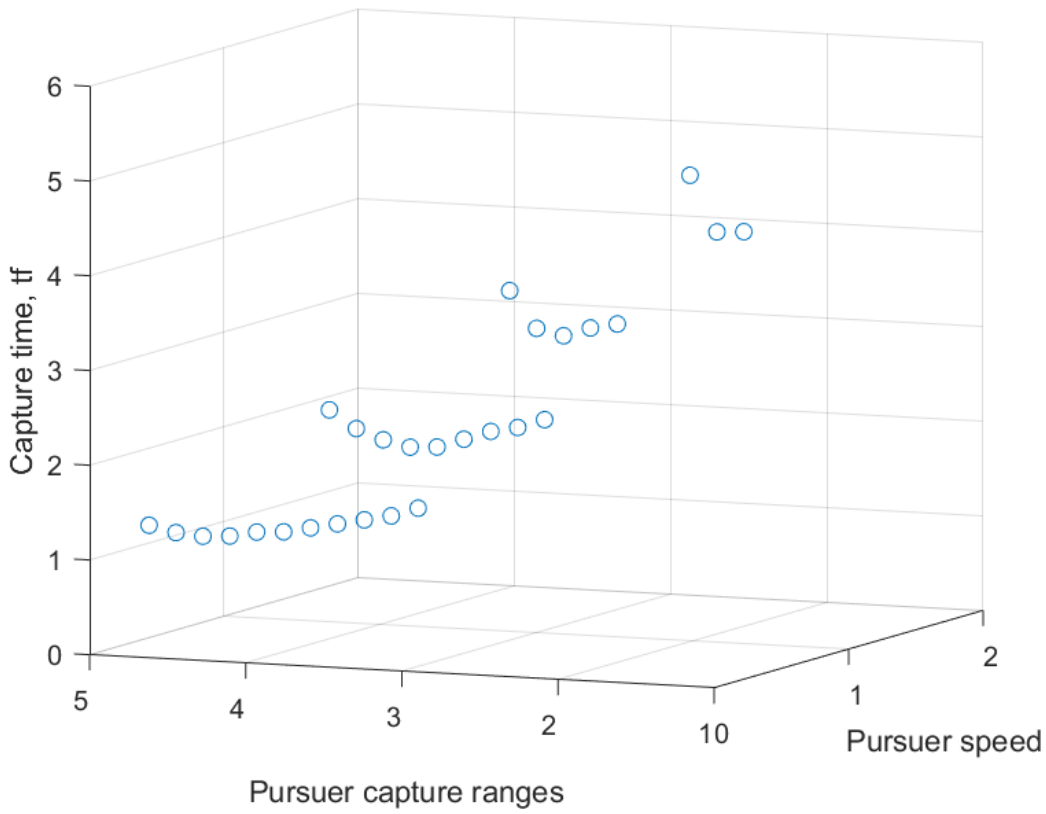


Figure 7: Equidistant pursuers: Capture time $t_f$ as function of capture range and speed

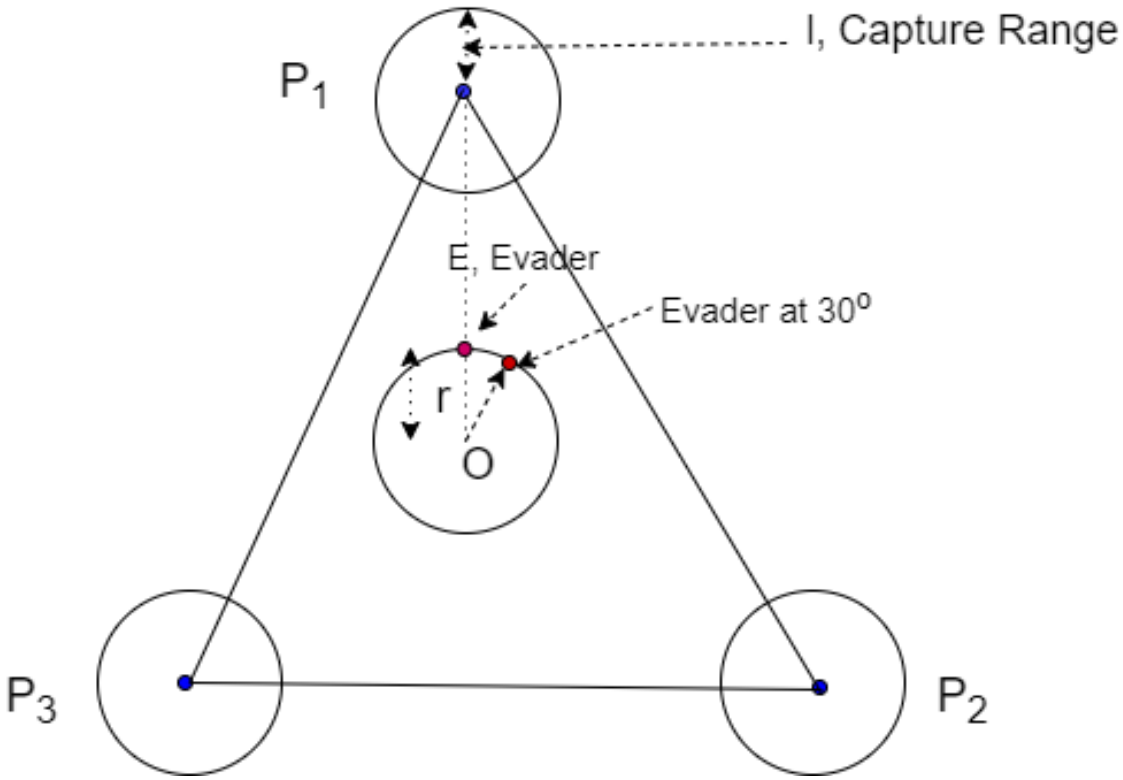


Figure 8: E initially on radial $OP_1$

#### 4.1.1.2 Evader, $E$ at line $OP_1$

$E$ is on the circumference of the circle of radius, $r$ whose center is $O$ of the equilateral triangle (see figure 8). The evaders escape by selecting the biggest escape cone -see equation 29. Capture times $t_f$ were collected, for the given speed ($\mu$), capture range ($l$) and radius ($r$) - see Table 2 - 4. The tables show that $t_f$ reduces with increasing speed, capture range or radius.

Table 2: $OP_1$ at $r = 0.1$

| **Evader Speed** | **Pursuer's capture range as fraction of the initial length of the triangle's side** | | | |
|---|---|---|---|---|
| $\mu$ | 20 % | 40 % | 60 % | 80 % |
| 0.000 | 5.360 | 3.960 | 2.640 | 1.280 |
| 0.200 | 4.840 | 3.600 | 2.440 | 1.160 |
| 0.400 | 4.800 | 3.480 | 2.240 | 1.080 |
| 0.600 | Escaped | 3.400 | 2.120 | 1.040 |
| 0.800 | Escaped | 3.440 | 2.040 | 0.960 |
| 1.000 | Escaped | Escaped | 2.080 | 0.920 |
| 1.200 | Escaped | Escaped | 2.000 | 0.880 |
| 1.400 | Escaped | Escaped | 1.960 | 0.840 |
| 1.600 | Escaped | Escaped | 1.920 | 0.800 |
| 1.800 | Escaped | Escaped | Escaped | 0.800 |
| 2.000 | Escaped | Escaped | Escaped | 0.760 |

Table 3: $OP_1$ at $r = 0.2$

| **Evader Speed** | **Pursuer's capture range as fraction of the initial length of the triangle's side** | | | |
|---|---|---|---|---|
| $\mu$ | 20 % | 40 % | 60 % | 80 % |
| 0.000 | 5.280 | 3.880 | 2.520 | 1.160 |
| 0.200 | 4.840 | 3.600 | 2.360 | 1.080 |
| 0.400 | 4.880 | 3.480 | 2.240 | 1.000 |
| 0.600 | Escaped | 3.400 | 2.120 | 0.960 |
| 0.800 | Escaped | 3.440 | 2.040 | 0.880 |
| 1.000 | Escaped | Escaped | 2.040 | 0.840 |
| 1.200 | Escaped | Escaped | 2.000 | 0.840 |
| 1.400 | Escaped | Escaped | 1.920 | 0.800 |
| 1.600 | Escaped | Escaped | 2.280 | 0.760 |
| 1.800 | Escaped | Escaped | Escaped | 0.720 |
| 2.000 | Escaped | Escaped | Escaped | 0.720 |

Table 4: $OP_1$ at $r = 0.3$

| **Evader Speed** | **Pursuer's capture range as fraction of the initial length of the triangle's side** | | | |
|---|---|---|---|---|
| $\mu$ | 20 % | 40 % | 60 % | 80 % |
| 0.000 | 5.240 | 3.760 | 2.400 | 1.040 |
| 0.200 | 4.800 | 3.600 | 2.280 | 0.960 |
| 0.400 | Escaped | 3.480 | 2.240 | 0.920 |
| 0.600 | Escaped | 3.400 | 2.120 | 0.880 |
| 0.800 | Escaped | 3.560 | 2.040 | 0.840 |
| 1.000 | Escaped | Escaped | 2.040 | 0.800 |
| 1.200 | Escaped | Escaped | 2.000 | 0.760 |
| 1.400 | Escaped | Escaped | 2.080 | 0.720 |
| 1.600 | Escaped | Escaped | 2.200 | 0.720 |
| 1.800 | Escaped | Escaped | Escaped | 0.680 |
| 2.000 | Escaped | Escaped | Escaped | 0.680 |

#### 4.1.1.3 $E$ at line $OP_1$ displaced by 30 degrees

Here the evader, E is on the circumference on the circle of radius, $r$ and the radial $OE$ is displaced by 30 degrees from its initial location (see Figure 8) while the distance between each pursuer is 10 units. Capture times $t_f$ were collected, for the given speed ($\mu$), capture range ($l$) and radius ($r$) (see Table 5-7) in a MATLAB simulation. Dynamic breakout gap detection (by selecting the appropriate escape cone) was also the mode of escape for the evader in this simulation. Our result found that the most favorable parameters of escape was a high evader speed, a low pursuer capture range and a high value for the evader circle radius, $r$.

Table 5: 30 degrees from $OP_1$ at $r = 0.1$

| **Evader Speed** | **Pursuer's capture range as fraction of the initial length of the triangle's side** | | | |
|---|---|---|---|---|
| $\mu$ | 20 % | 40 % | 60 % | 80 % |
| 0.000 | 5.320 | 4.000 | 2.640 | 1.320 |
| 0.200 | 4.800 | 3.560 | 2.400 | 1.200 |
| 0.400 | 4.840 | 3.480 | 2.200 | 1.120 |
| 0.600 | Escaped | 3.360 | 2.080 | 1.040 |
| 0.800 | Escaped | 3.320 | 2.000 | 0.960 |
| 1.000 | Escaped | Escaped | 2.080 | 0.920 |
| 1.200 | Escaped | Escaped | 2.080 | 0.880 |
| 1.400 | Escaped | Escaped | 2.040 | 0.840 |
| 1.600 | Escaped | Escaped | 2.120 | 0.800 |
| 1.800 | Escaped | Escaped | Escaped | 0.760 |
| 2.000 | Escaped | Escaped | Escaped | 0.720 |

Table 6: 30 degrees from $OP_1$ at $r = 0.2$

| **Evader Speed** | **Pursuer's capture range as fraction of the initial length of the triangle's side** | | | |
|---|---|---|---|---|
| $\mu$ | 20 % | 40 % | 60 % | 80 % |
| 0.000 | 5.240 | 3.960 | 2.600 | 1.200 |
| 0.200 | 4.800 | 3.560 | 2.360 | 1.120 |
| 0.400 | 4.840 | 3.480 | 2.200 | 1.040 |
| 0.600 | Escaped | 3.360 | 2.080 | 1.000 |
| 0.800 | Escaped | 3.360 | 2.000 | 0.920 |
| 1.000 | Escaped | Escaped | 2.000 | 0.880 |
| 1.200 | Escaped | Escaped | 1.960 | 0.840 |
| 1.400 | Escaped | Escaped | 2.080 | 0.800 |
| 1.600 | Escaped | Escaped | 2.200 | 0.800 |
| 1.800 | Escaped | Escaped | Escaped | 0.760 |
| 2.000 | Escaped | Escaped | Escaped | 0.720 |

Table 7: 30 degree from $OP_1$ at $r = 0.3$

| **Evader Speed** | **Pursuer's capture range as fraction of the initial length of the triangle's side** | | | |
|---|---|---|---|---|
| $\mu$ | 20 % | 40 % | 60 % | 80 % |
| 0.000 | 5.160 | 3.920 | 2.520 | 1.120 |
| 0.200 | 4.760 | 3.520 | 2.360 | 1.040 |
| 0.400 | Escaped | 3.440 | 2.200 | 0.960 |
| 0.600 | Escaped | 3.320 | 2.080 | 0.920 |
| 0.800 | Escaped | 3.480 | 2.000 | 0.880 |
| 1.000 | Escaped | Escaped | 2.080 | 0.840 |
| 1.200 | Escaped | Escaped | 2.040 | 0.800 |
| 1.400 | Escaped | Escaped | 1.920 | 0.760 |
| 1.600 | Escaped | Escaped | Escaped | 0.760 |
| 1.800 | Escaped | Escaped | Escaped | 0.720 |
| 2.000 | Escaped | Escaped | Escaped | 0.720 |

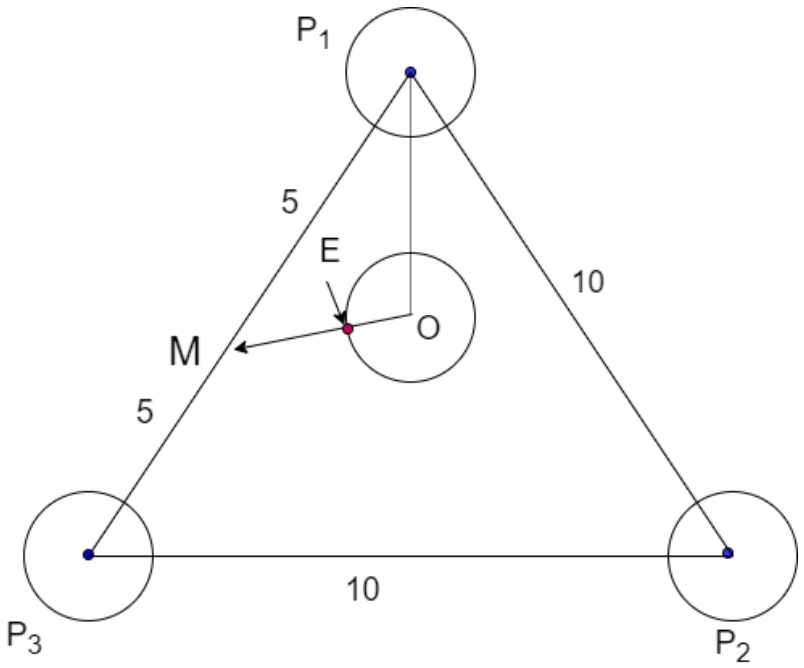


Figure 9: E initially on segment OM

#### 4.1.1.4 $E$ at line $OM$

$E$ is initially on line $OM$, where $M$ is the midpoint of the side $P_1P_3$ of the equilateral triangle shown in fig 9. The angle $< MOP_1$ needs to be determined to run the simulation for this problem in MATLAB. The equilateral triangle has length of 10 on all sides, $\overline{OP_1} = \frac{5}{\sqrt{3}}$.

To solve for $< MOP_1$ in fig 9 solve for line $OM$ which is a 'Side Angle Side' problem (SAS) in trigonometry.
Using the Law of cosines
$\overline{OM}^2 = 5^2 + (\frac{5}{\sqrt{3}})^2 - 2 \times 5 \times \frac{5}{\sqrt{3}} \cos 30$

$\overline{OM}^2 = 25 + \frac{25}{3} - \frac{50}{\sqrt{3}} \cos 30$

$\overline{OM} = 2.886751$

Apply the 'Law of sine' to get closer to a solution for $< MOP_1$ by selecting the smaller of the two remaining unknown angles, $< P_1MO$

$\frac{\sin 30}{2.886751} = \frac{\sin(<P_1MO)}{\frac{5}{\sqrt{3}}}$

$\frac{\sin 30}{2.886751} = \frac{\sqrt{3} \times \sin(<P_1MO)}{5}$

$\sin(< P_1MO) = \frac{5 \times \sin 30}{2.886751 \times \sqrt{3}}$

$< P_1MO = 29.9999^0 \approxeq 30^0$

$< MOP_1 = 180^0 - < P_1MO - < OP_1M$

$< MOP_1 = 180^0 - 30^0 - 30^0 = 120^0$

Conduct a simulation in MATLAB (using the derived value of $< MOP_1$) to measure $t_f$s for varied values of $\mu, l, r$. High evader speed, low pursuer capture range and high evader radius gave the best outcome for the evader's chances of escape. Results are shown in Table(8-10).

Table 8: E on line OM at $r = 0.1$

| **Evader Speed** | **Pursuer's capture range as fraction of the initial length of the triangle's side** | | | |
|---|---|---|---|---|
| $\mu$ | 20 % | 40 % | 60 % | 80 % |
| 0.000 | 5.360 | 3.960 | 2.640 | 1.280 |
| 0.200 | 4.720 | 3.600 | 2.440 | 1.160 |
| 0.400 | 4.680 | 3.480 | 2.240 | 1.080 |
| 0.600 | Escaped | 3.440 | 2.120 | 1.040 |
| 0.800 | Escaped | 3.520 | 2.040 | 0.960 |
| 1.000 | Escaped | Escaped | 2.080 | 0.920 |
| 1.200 | Escaped | Escaped | 2.040 | 0.880 |
| 1.400 | Escaped | Escaped | 1.960 | 0.840 |
| 1.600 | Escaped | Escaped | 1.920 | 0.800 |
| 1.800 | Escaped | Escaped | Escaped | 0.800 |
| 2.000 | Escaped | Escaped | Escaped | 0.760 |

Table 9: E on line OM at $r = 0.2$

| **Evader Speed** | **Pursuer's capture range as fraction of the initial length of the triangle's side** | | | |
|---|---|---|---|---|
| $\mu$ | 20 % | 40 % | 60 % | 80 % |
| 0.000 | 5.280 | 3.880 | 2.520 | 1.160 |
| 0.200 | 4.720 | 3.600 | 2.360 | 1.080 |
| 0.400 | 4.720 | 3.480 | 2.280 | 1.000 |
| 0.600 | Escaped | 3.440 | 2.040 | 0.880 |
| 0.800 | Escaped | 3.440 | 2.040 | 0.880 |
| 1.000 | Escaped | Escaped | 2.040 | 0.840 |
| 1.200 | Escaped | Escaped | 2.040 | 0.800 |
| 1.400 | Escaped | Escaped | 1.920 | 0.800 |
| 1.600 | Escaped | Escaped | 2.240 | 0.760 |
| 1.800 | Escaped | Escaped | Escaped | 0.720 |
| 2.000 | Escaped | Escaped | Escaped | 0.720 |

Table 10: E on line OM at $r = 0.3$

| **Evader Speed** | **Pursuer's capture range as fraction of the initial length of the triangle's side** | | | |
|---|---|---|---|---|
| $\mu$ | 20 % | 40 % | 60 % | 80 % |
| 0.000 | 5.240 | 3.760 | 2.400 | 1.040 |
| 0.200 | 4.720 | 3.640 | 2.280 | 0.960 |
| 0.400 | 4.920 | 3.520 | 2.240 | 0.920 |
| 0.600 | Escaped | 3.440 | 2.120 | 0.880 |
| 0.800 | Escaped | 3.640 | 2.040 | 0.840 |
| 1.000 | Escaped | Escaped | 2.080 | 0.800 |
| 1.200 | Escaped | Escaped | 2.040 | 0.760 |
| 1.400 | Escaped | Escaped | 2.080 | 0.720 |
| 1.600 | Escaped | Escaped | 2.200 | 0.720 |
| 1.800 | Escaped | Escaped | Escaped | 0.680 |
| 2.000 | Escaped | Escaped | Escaped | 0.680 |

### 4.1.2 Non-Equidistant Pursuers

A cyclic pursuit scenario was created shown in figure 10 with non-equidistant spaced pursuers of distances 20, 20, $3\sqrt{30}$. During this cyclic pursuit, two pursuers ($P_1$ and $P_2$) come together then they both coalesce with the third pursuer ($P_3$). See Fig 3 and 11 The initial capture range, $l$, was ranging from 20% (1.9664 units) range to 80% (7.8655 units) in 20% increments. 100% capture range is defined as the distance from any of the pursuers to the evader at time $dt = 0$ Simulations using MATLAB( see Table 11-13) were performed with dynamic breakout gap detection, varying speed and capture range to see if the evader, E escapes and if not how long $t_f$ it takes to capture the evader. The breakout gap at every discretized time $dt$ was always the escape cone with the biggest angle (see Strategy section). The evader initial state region was located on the circumference of a circle centered in triangular encirclement. The radius, $r$ of this circumference was varied during the simulation. The analysis of the result was to detect a pattern in the relationship between any of the varied parameters. The results showed that at a given speed, an increasing $l$ resulted in a decreasing in $t_f$.

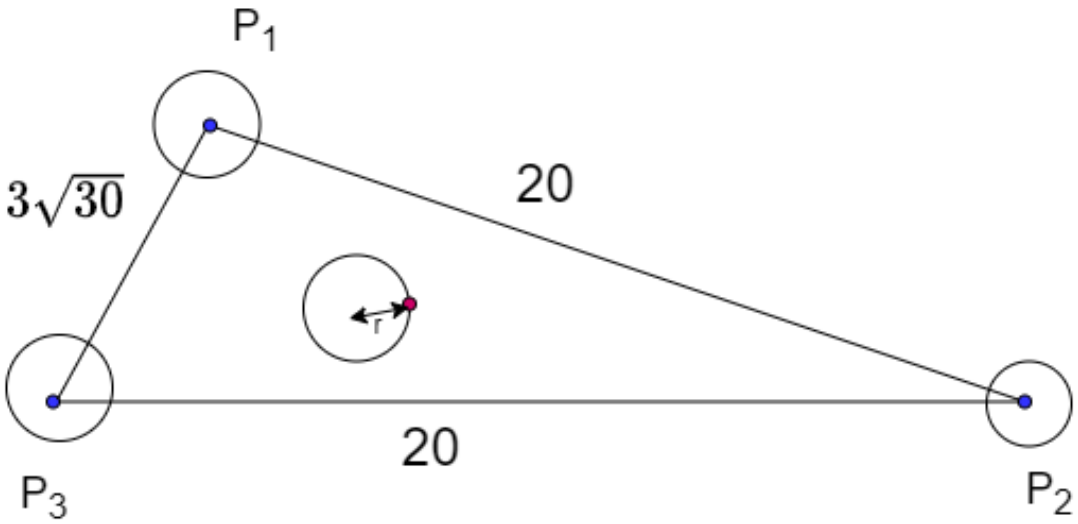


Figure 10: Non equidistant Pursuers

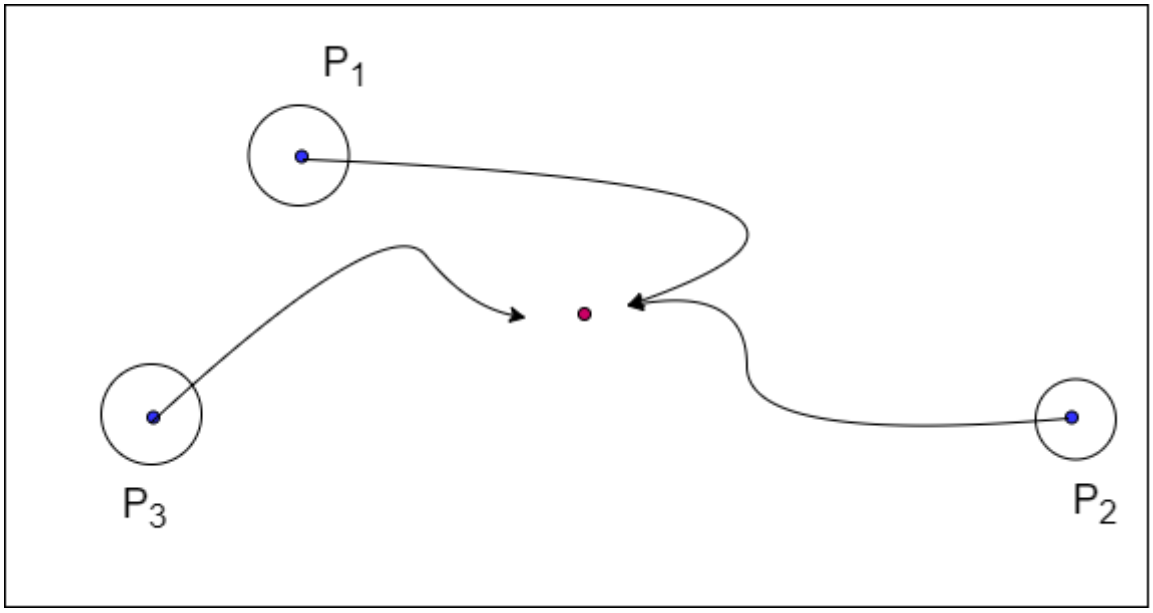


Figure 11: Non Equidistant Pursuers trajectory

Table 11: Non-Equidistant Pursuit with E at $r = 0.1$

| **Evader Speed** | **Pursuer's capture range as fraction of the initial length of the triangle's side** | | | |
|---|---|---|---|---|
| $\mu$ | 20 % | 40 % | 60 % | 80 % |
| 0.000 | 10.960 | 8.120 | 5.520 | 2.800 |
| 0.100 | 10.360 | 7.880 | 5.560 | 3.240 |
| 0.300 | 10.040 | 7.560 | 5.320 | 3.240 |
| 0.500 | Escaped | 8.160 | 5.400 | 3.160 |
| 0.700 | Escaped | Escaped | 5.840 | 3.120 |
| 0.900 | Escaped | Escaped | 7.000 | 3.160 |
| 1.100 | Escaped | Escaped | Escaped | 3.440 |
| 1.300 | Escaped | Escaped | Escaped | 3.480 |
| 1.500 | Escaped | Escaped | Escaped | 3.600 |
| 1.700 | Escaped | Escaped | Escaped | 3.480 |
| 1.900 | Escaped | Escaped | Escaped | Escaped |
| 2.100 | Escaped | Escaped | Escaped | Escaped |

Table 12: Non-Equidistant Pursuit with E at $r = 0.3$

| **Evader Speed** | **Pursuer's capture range as fraction of the initial length of the triangle's side** | | | |
|---|---|---|---|---|
| $\mu$ | 20 % | 40 % | 60 % | 80 % |
| 0.000 | 10.640 | 8.040 | 5.760 | 3.080 |
| 0.100 | 9.800 | 7.680 | 5.520 | 3.440 |
| 0.300 | 10.120 | 7.640 | 5.320 | 3.280 |
| 0.500 | Escaped | 8.200 | 5.480 | 3.200 |
| 0.700 | Escaped | Escaped | 5.920 | 3.160 |
| 0.900 | Escaped | Escaped | Escaped | 3.200 |
| 1.100 | Escaped | Escaped | Escaped | 3.440 |
| 1.300 | Escaped | Escaped | Escaped | 3.480 |
| 1.500 | Escaped | Escaped | Escaped | 3.440 |
| 1.700 | Escaped | Escaped | Escaped | Escaped |
| 1.900 | Escaped | Escaped | Escaped | Escaped |
| 2.100 | Escaped | Escaped | Escaped | Escaped |

Table 13: Non-Equidistant Pursuit with E at $r = 0.5$

| **Evader Speed** | **Pursuer's capture range as fraction of the initial length of the triangle's side** | | | |
|---|---|---|---|---|
| $\mu$ | 20 % | 40 % | 60 % | 80 % |
| 0.000 | 10.400 | 7.960 | 5.720 | 3.360 |
| 0.100 | 9.760 | 7.640 | 5.520 | 3.440 |
| 0.300 | 10.320 | 7.720 | 5.360 | 3.280 |
| 0.500 | Escaped | 8.400 | 5.640 | 3.200 |
| 0.700 | Escaped | Escaped | 5.960 | 3.200 |
| 0.900 | Escaped | Escaped | Escaped | 3.280 |
| 1.100 | Escaped | Escaped | Escaped | 3.520 |
| 1.300 | Escaped | Escaped | Escaped | 3.480 |
| 1.500 | Escaped | Escaped | Escaped | 3.600 |
| 1.700 | Escaped | Escaped | Escaped | Escaped |
| 1.900 | Escaped | Escaped | Escaped | Escaped |
| 2.100 | Escaped | Escaped | Escaped | Escaped |

## 4.2 Temporal evolution of distance

#### 4.2.0.1 Analysis

Considering the following scenarios in which $\triangle P_1P_2P_3$ is formed by pursers in an acute triangle formation in the pattern of figure 5. Plots (figures 12 - 31) were generated from several experiments using equation (33). For the acute triangle formations plotted in figure 12 & 13, we see that curves $r_1, r_2$, and $r_3$ decline from their initial distance over time. We also see that that $r_1$ and $r_2$ cross first. When the two curves cross, the given triangle formation becomes isosceles. After this occurrence, $r_2$'s value continues to decline until it becomes a very small value and then it holds steady for a while before eventually becoming zero. While $r_2$ holds a steady value over time, $r_1$ and $r_3$ almost coalesce but they do not, they get very close and together decline at about the same slope. $r_3$ goes down to 0. When $r_3$ gets to zero, $r_1$ and $r_2$ coalesce and decline to 0 as well. This results in two pursuers merging into one and both pursuers($P_1$ and $P_2$ ) advance together to meet the third pursuer ($P_3$) head on.

For the acute triangle formations plotted in figures 14 & 15, curves $r_1, r_2$, and $r_3$ decline from their initial distance as time increases. Curves $r_3$ and $r_2$ cross, this means $r_2$ and $r_3$ reached the same distance at the time. As all the 3 'r's continue to decline in distance as the pursuit goes on, $r_2$ crosses $r_1$. Next $r_1$ and $r_3$ coalesce at the exact time that $r_2$ goes to 0. What happens here is pursuers $P_1$ and $P_3$ coalesce and approach $P_2$ head on.

Considering a different scenario in which $\triangle P_1P_2P_3$ is formed by pursers in an obtuse triangle formation in the pattern of figure 5. For the obtuse triangle formations plotted in figure 16, we see, $r_1$ , $r_2$ and $r_3$ decline overtime in this graph, curves $r_2$ and $r_3$ cross first. When this happens $r_2$ and $r_3$ have the same value at that point. Curves $r_1$ , $r_2$ and $r_3$ continue to decline, $r_2$ now crosses $r_1$, while $r_1$ and $r_2$ now $\gg$ $r_3$. $r_1$ and $r_2$ continue to decline at the same gradient and maintain close values. $r_3$

continues to decline but gets close to zero and holds the values for some time. $r_3$ crosses $r_1$ then coalesces with $r_2$ exactly when $r_1$ goes to 0. Next $r_2$ and $r_3$ gradually reduces to 0. Figure 17 is quite similar to figure 16 in its analysis except for the fact that $r_1$ and $r_2$ cross sooner, it is also a plot of obtuse triangle formation of pursuers. Also when $r_1$ and $r_2$ continue to decline at the same gradient and maintain close values just like in figure 16, but both $r_1$ and $r_2$ are less closer to each other. For both cases (figure 16 & figure 17), pursuers $P_1$ and $P_3$ coalesce and approach $P_2$ head on. If we analyze figures 18 & 19 , we see in both scenarios $r_1, r_2$, and $r_3$ continue to decline in their respective value during the pursuit. Next $r_2$ crosses $r_3$. When this happens $r_3$ continues to decline all the way down to 0. At the exact time that $r_3$ reaches 0 $r_2$ has coalesced with $r_1$, $r_1$ & $r_2$ now begin a journey down to a value of 0. The dynamics here is simply that $P_1$ and $P_2$ have coalesced which has resulted in $r_3$ going to 0. Next $P_3$ approaches $P_1$ and $P_2$, $P_1$ and $P_2$ approaches $P_3$. This dynamic results in a head on train wreck scenario.

Finally, considering a special case in which $\triangle P_1P_2P_3$ is formed by pursers in an equilateral triangle formation in the pattern of figure 5. In this case, the pursuers have the same initial value for $r$ and they come together at the same time. The rate of decline of $r_1$, $r_2$ & $r_3$ is the same and they all reach 0 at the same time. See figures 20 & 21 -the plots reveal that $r_1$, $r_2$ & $r_3$ are superimposed, with $r_3$ only shown because it is the last of the three $r$s plotted for each case. The results show that indeed the proposition described in this section is true. Plots (figures 12 - 31) experimentally validate the proposition. For the non-equilateral cases, we see several times in which smaller isosceles triangles were generated during the temporal evolution process. This resulted in two pursuers coming together forming a cluster in a head on encounter with a third pursuer whereupon all three pursuers ended up coming together. In all cases the three pursuers came together in finite time.

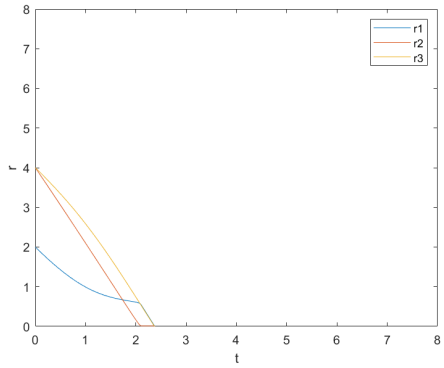


Figure 12: Temporal evolution of lengths of sides 2, 4, 4

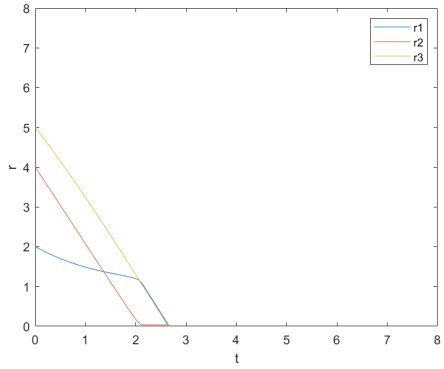


Figure 13: Temporal evolution of lengths of sides 2,4,5

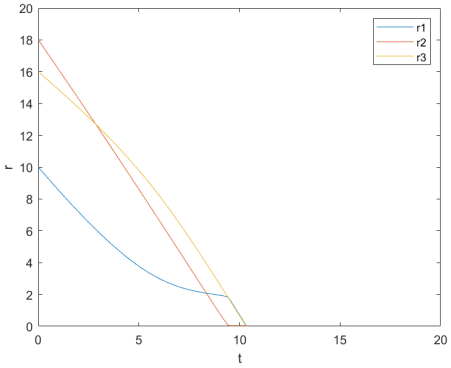


Figure 14: Temporal evolution of lengths of sides 10, 18, 16

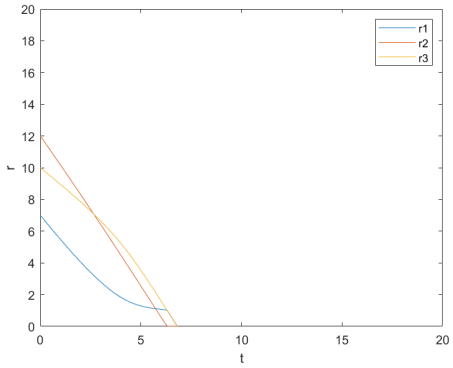


Figure 15: Temporal evolution of lengths of sides 7, 12, 10

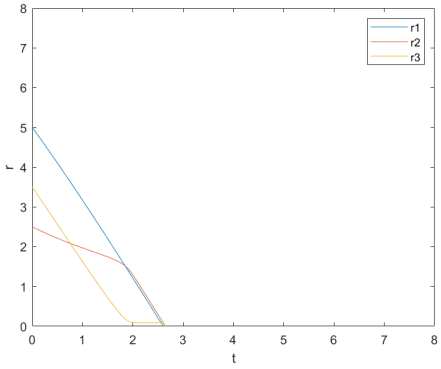


Figure 16: Temporal evolution of lengths of sides 5,2.5,3.5

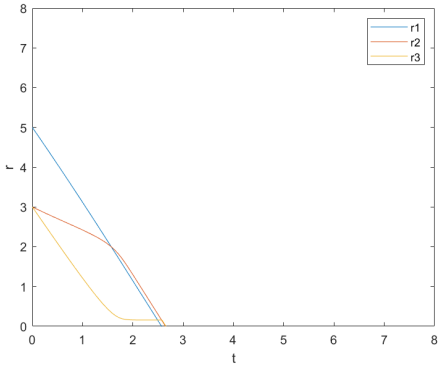


Figure 17: Temporal evolution of lengths of sides 5,3,3

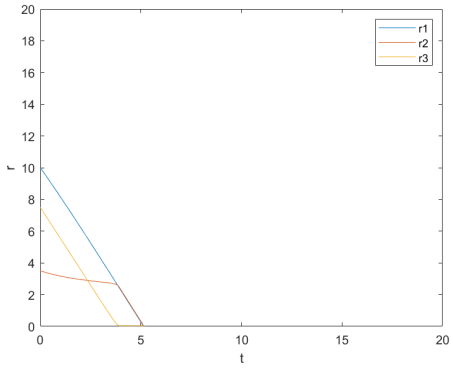


Figure 18: Temporal evolution of lengths of sides 10, 3.5, 7.5

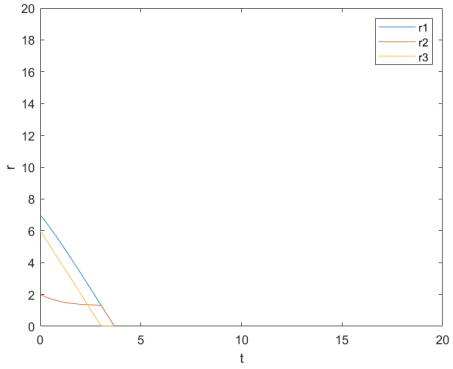


Figure 19: Temporal evolution of lengths of sides 7, 2, 6

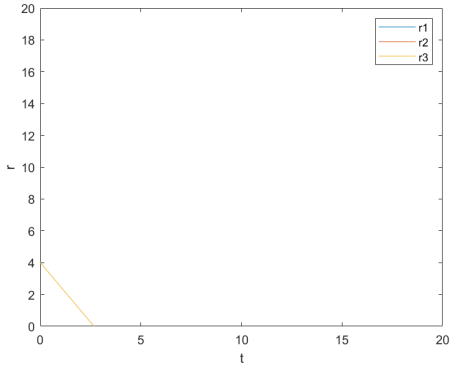


Figure 20: Temporal evolution of lengths of sides 4, 4, 4

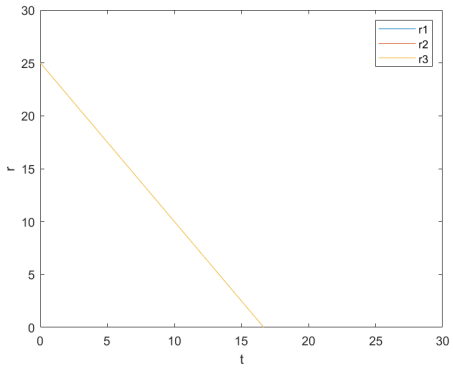


Figure 21: Temporal evolution of lengths of sides 25, 25, 25

Let us consider the triangle $\triangle P_1P_2P_3$ in figure 5 to represent the location of three pursuers in cyclic pursuit. The pursuers positions are connected to form a triangle for each case (see figures 22 - 31 ). For the equidistant pursuers it results in an equilateral triangle. For the non-equidistant pursuers, the focus was on acute and obtuse triangle formations. In all cases the triangles shrunk overtime as expected. The animation was generated by plotting the positions of the three pursuers and each given time, dt -using Euler's method. The plots are to show the details of convergence for all the cases. For each case, there is a plot for smaller time step scenario and one for bigger time step scenario to show progression. For the acute and obtuse triangles, a straight line is shown inside the innermost triangle. This is representative of the process in which two pursuers come together to collide head-on with the third pursuer. This straight line approximates the head on collision path. For the equilateral triangle, the triangle shrinks at the same rate it remains equilateral until it coalesces to the center of the triangle at the very end. The three pursuers in this case arrive at the center at the same time. The collective results validate the preposition.

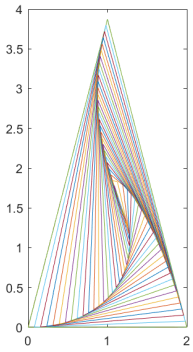


(a) Shrinking temporal lenghts for sides 2, 4, 4, in small time steps

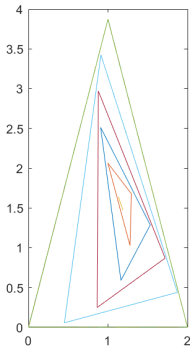


(b) Shrinking temporal lenghts for sides 2, 4, 4 in big time steps

Figure 22: Shrinking temporal lenghts for sides 2, 4, 4

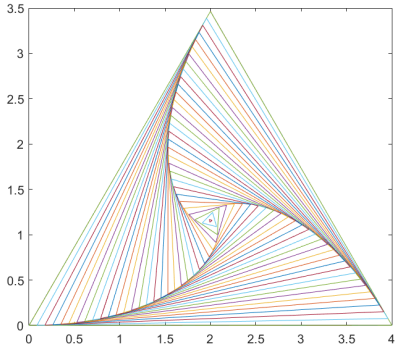


(a) Shrinking temporal lenghts for sides 4, 4, 4, in small time steps

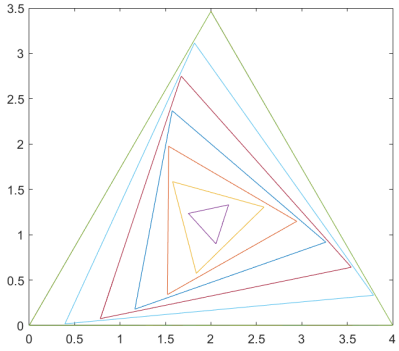


(b) Shrinking temporal lenghts for sides 4, 4, 4 in big time steps

Figure 23: Shrinking temporal lenghts for sides 4, 4, 4

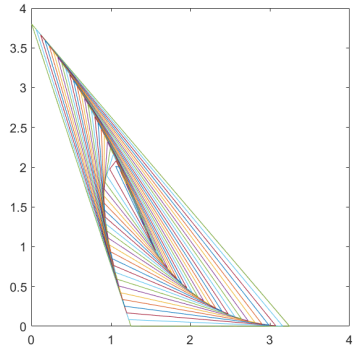


(a) Shrinking temporal lenghts for sides 2, 4, 5, in small time steps

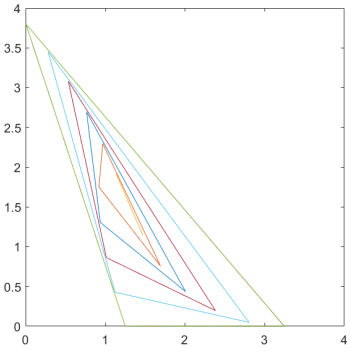


(b) Shrinking temporal lenghts for sides 2, 4, 5 in big time steps

Figure 24: Shrinking temporal lenghts for sides 2, 4, 5

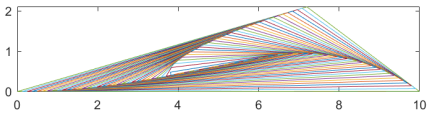


(a) Shrinking temporal lenghts for sides 10, 3.5, 7.5 in small time steps

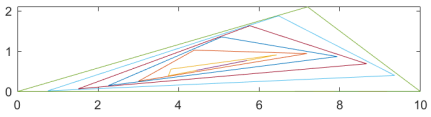


(b) Shrinking temporal lenghts for sides 10, 3.5, 7.5 in big time steps

Figure 25: Shrinking temporal lenghts for sides 10, 3.5, 7.5

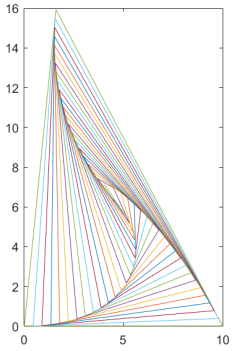


(a) Shrinking temporal lenghts for sides 10, 18, 16 in small time steps

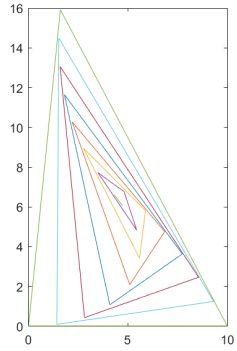


(b) Shrinking temporal lenghts for sides 10, 18, 16 in big time steps

Figure 26: Shrinking temporal lenghts for sides 10, 18, 16

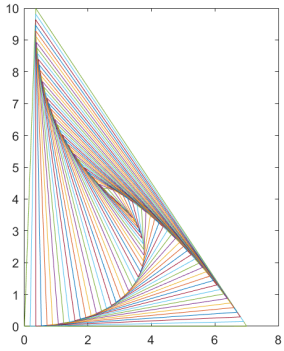


(a) Shrinking temporal lenghts for sides 7, 12, 10 in small time steps

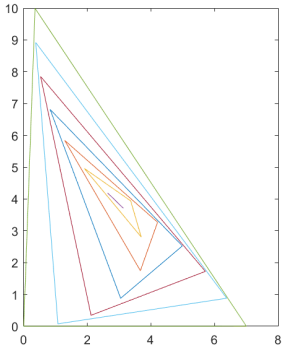


(b) Shrinking temporal lenghts for sides 7, 12, 10 in big time steps

Figure 27: Shrinking temporal lenghts for sides 7, 12, 10

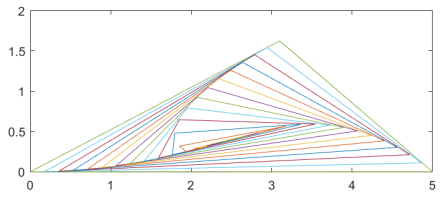


(a) Shrinking temporal lenghts for sides 5, 2.5, 3.5, in small time steps

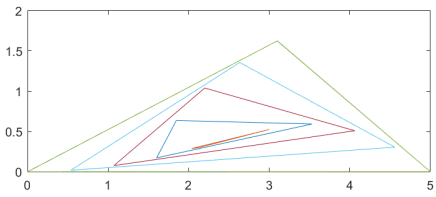


(b) Shrinking temporal lenghts for sides 5, 2.5, 3.5 in big time steps

Figure 28: Shrinking temporal lenghts for sides 5, 2.5, 3.5

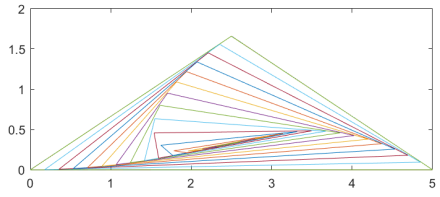


(a) Shrinking temporal lenghts for sides 5, 3, 3 in small time steps

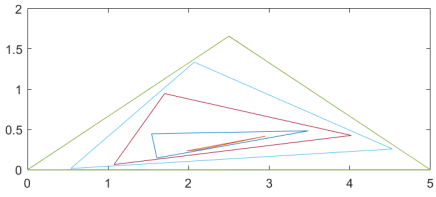


(b) Shrinking temporal lenghts for sides 5, 3, 3 in big time steps

Figure 29: Shrinking temporal lenghts for sides 5, 3, 3

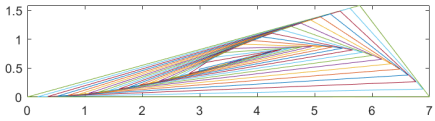


(a) Shrinking temporal lenghts for sides 7, 2, 6 in small time steps

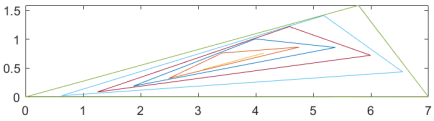


(b) Shrinking temporal lenghts for sides 7, 2, 6 in big time steps

Figure 30: Shrinking temporal lenghts for sides 7, 2, 6

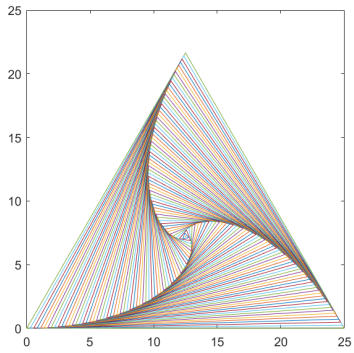


(a) Shrinking temporal lenghts for sides 25, 25, 25 in small time steps

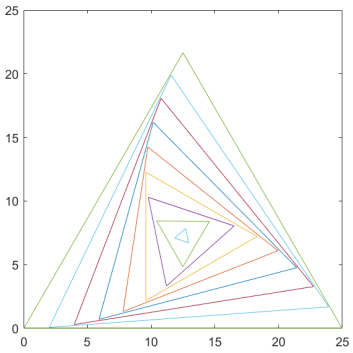


(b) Shrinking temporal lenghts for sides 25, 25, 25 in big time steps

Figure 31: Shrinking temporal lenghts for sides 25, 25, 25

### 4.3 Shrinking n-gon Analysis and Results

Let us consider the trapezoid $\overline{P_1P_2P_3P_4}$ in figure 32 The figure represents four pursuers spaced in the shape of a trapezoid in cyclic pursuit. In this case we have a polygon with different side lengths. According to the preposition (see Methodology chapter 3.3.2.1), cyclic pursuit over some time will result in the number of sides decreasing by one gradually until we have a straight line converging into a single point located at the center of the original shape. An experiment was conducted to verify this proposition. The result of the simulation conducted in MATLAB validates that the proposition is true -see figure 33. Figure 33(a) basically just shows the trajectory over time of the trapezoid from its original size until its final convergence at the center of figure. Figure 33(b) zooms in a few frames just before the number of sides begin to reduce by one each time. The trapezoid reduces into a triangle then a straight line and eventually converges to a point.

Consider the quadrangle $\overline{P_1P_2P_3P_4}$ in figure 34, it represents for pursuers spaced in rectangular form in cyclic pursuit. Over time (see figure 35) the pursuers spacing shrinks into smaller rectangles until it becomes a small line which in turn become a bold point at the center of the figure. The small line eventually converges in the center of the figure representing the bold point in the center of the figure. The small line in the center reveals that at least one of the pursuers will collide with the rest of the pursuer head-on during convergence. The results obtained does not confirm the preposition since it did not change shape to a triangle formation before the line formation. The quadrangle $\overline{P_1P_2P_3P_4}$ in figure 36 represent four pursuers in cyclic pursuit spaced equidistanct from each other- in the formation of a square. The trajectory of the respective distances will shrink overtime while all four pursuers will remain equidistant. This will result in a shrinking square converging into a bold point

in the center of the figure. The bold point shown without a line is an indication that all four pursuers arrived at the center of the figure at the same time - see figure 37.

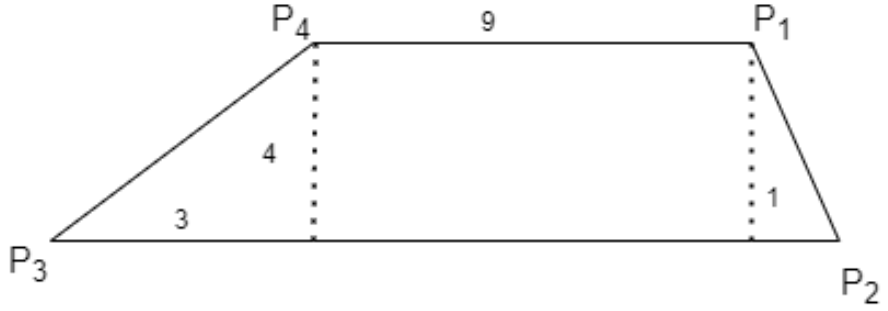


Figure 32: Trapezoid shaped spacing of pursuers

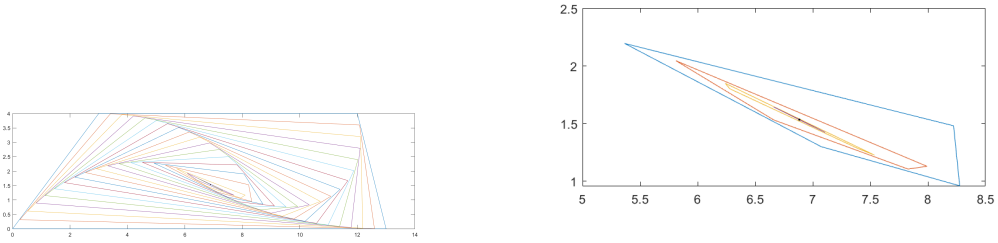


(a) Trajectory of trapezoid shaped spacing of pursuers

(b) Magnified trajectory of trapezoid shaped spacing of pursuers

Figure 33: Trajectory of trapezoid shaped spacing of pursuers


Figure 34: Rectangular shaped spacing of pursuers

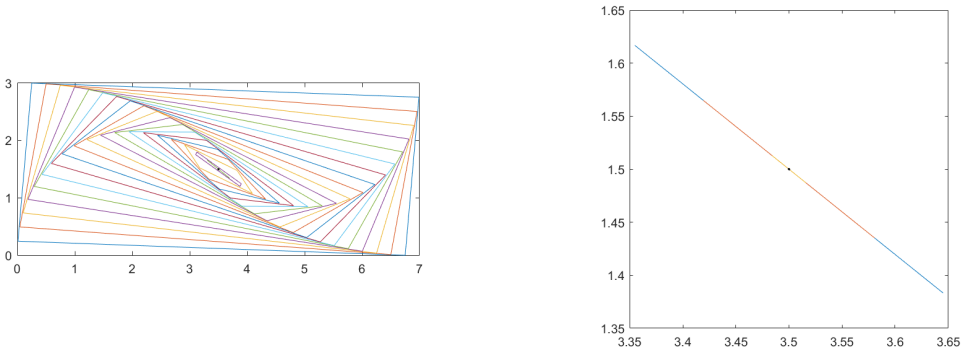


(a) Trajectory of rectanglar shaped spacing of pursuers

(b) Magnified trajectory of rectangular shaped spacing of pursuers

Figure 35: Trajectory of rectangular shaped spacing of pursuers

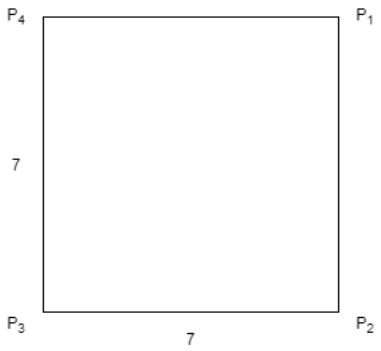


Figure 36: Square shaped spacing of pursuers

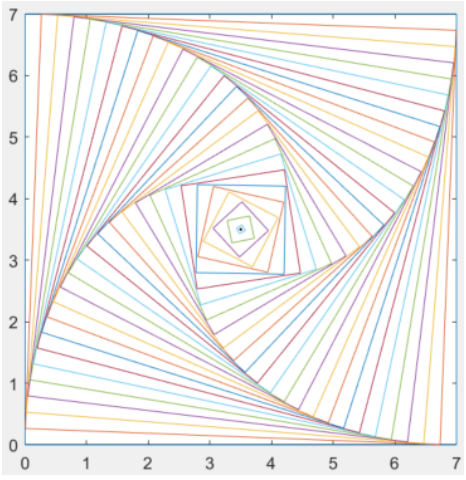


(a) Trajectory of square shaped spacing of pursuers

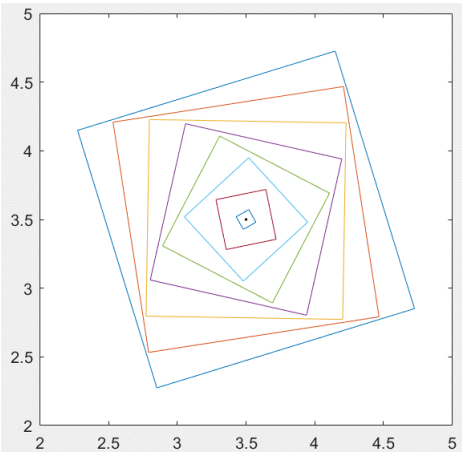


(b) Magnified trajectory of square shaped spacing of pursuers

Figure 37: Trajectory of square shaped spacing of pursuers

## 4.4 Capturability

#### 4.4.0.1 Analysis

By applying Euler's theory to equation 40, the following parameters were simulated and the results plotted:

1. $\mu = \frac{\sqrt{3}}{2}, r_o = 2.0, l = 1/2$
2. $\mu = \frac{1}{2}, r_o = 2.0, l = 1/2$
3. $\mu = \frac{1}{4}, r_o = 2.0, l = 1/2$
4. $\mu = \frac{4}{5}\sqrt{3}, r_o = 2.0, l = 3/4$
5. $\mu = \sqrt{3}, r_o = 2.0, l = 3/4$
6. $\mu = \sqrt{3}, r_o = 2.0, l = 1/4$

The parameters 1, 2, 4 and 5 all satisfy equation 37 - see corresponding plots in figures 38, 39, 41 and 42. Equation 37 helps determine the minimum speed for evasion at time $t_e^*$. The blue triangle is the shaped formed by the three pursuers at time instant $t_e^*$ . At minimum time $t_e^*$ the evader would have made it to the side $P_1P_3$ of the triangle formed. For cases where equation 37 is satisfied, the evader manages to escape encirclement at time $t_e^*$.

There is a distinction between escaping encirclement and escaping capture completely. Although the evader may escape encirclement at time $t_e^*$, the evader may be captured later on. The plots(Figures 38, 39 ,41 and 42 ) depict the evader escaping at time $t_e^*$ but being eventually captured at or before time $t_c$. Figure 40 does not satisfy equation 37 and it's plot depicts the evader captured before time $t_e^*$. Finally figure 43 is figure 42 with a reduced capture range in which the the evader escapes capture

at time $t_e^*$, $t_c$ and beyond until capture is no longer possible

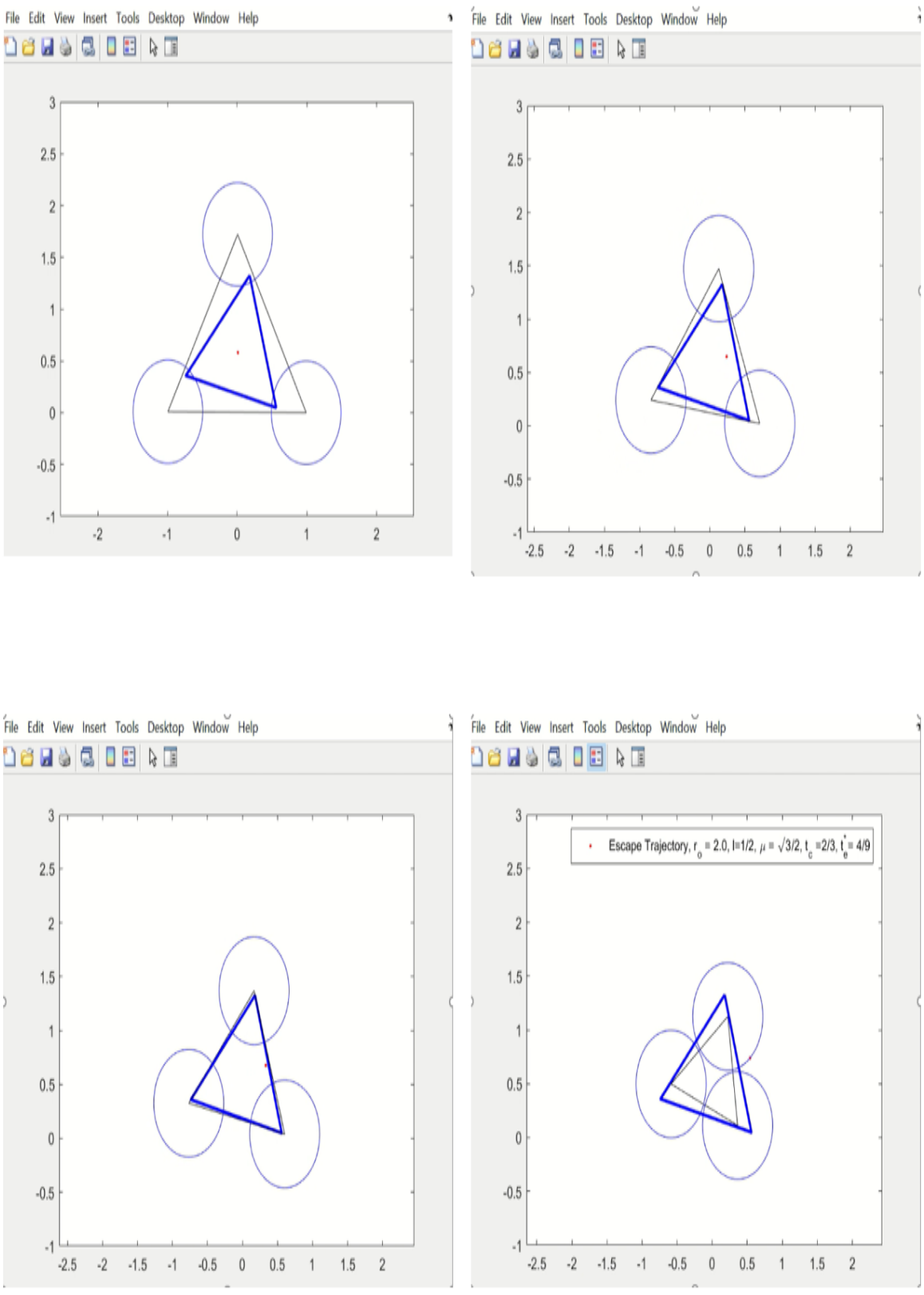


Figure 38: Equidistant pursuers: escape Trajectory, $\mu = \frac{\sqrt{3}}{2}, r_o = 2.0, l = 1/2$

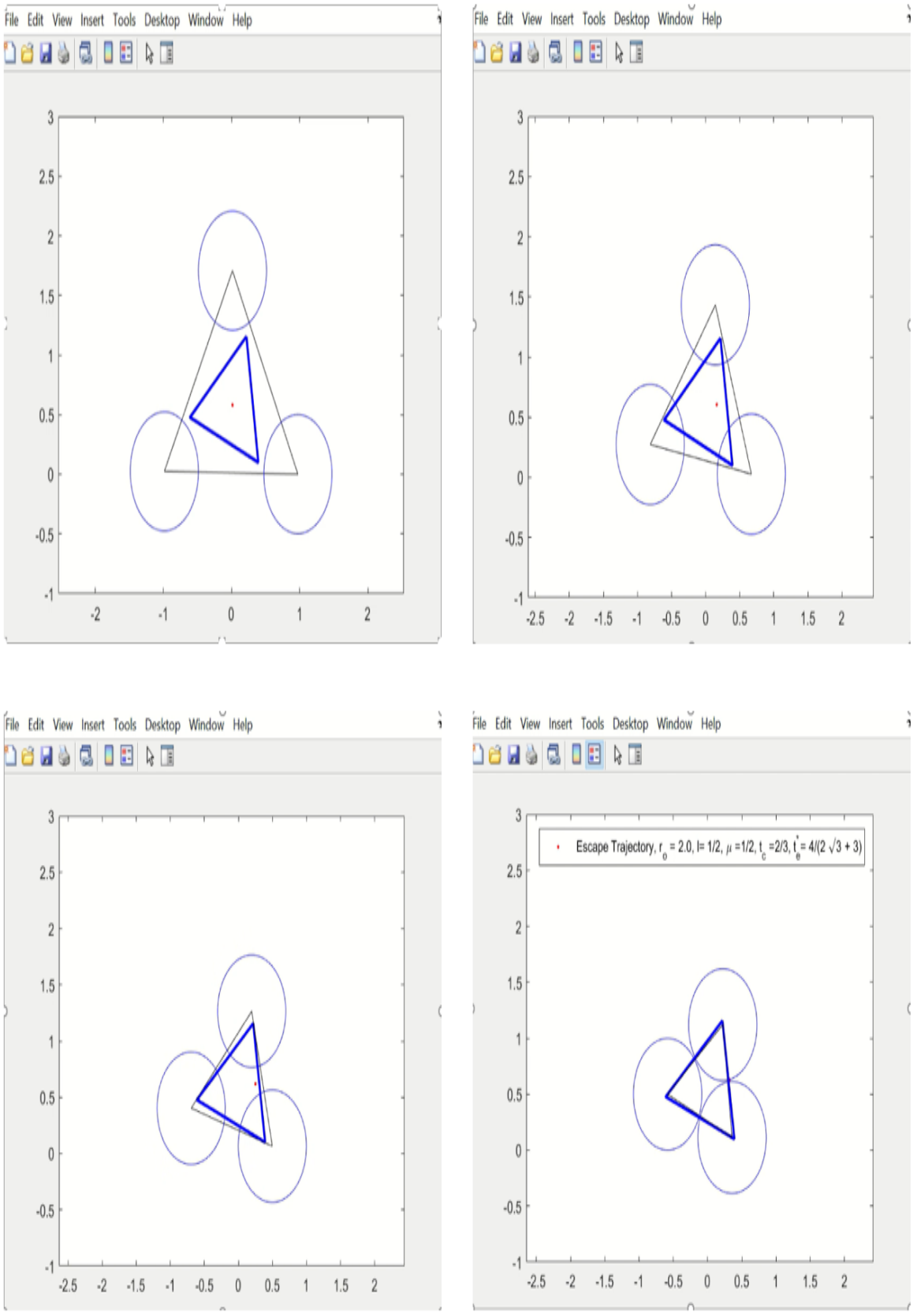


Figure 39: Equidistant pursuers: escape Trajectory, $\mu = \frac{1}{2}, r_o = 2.0, l = 1/2$

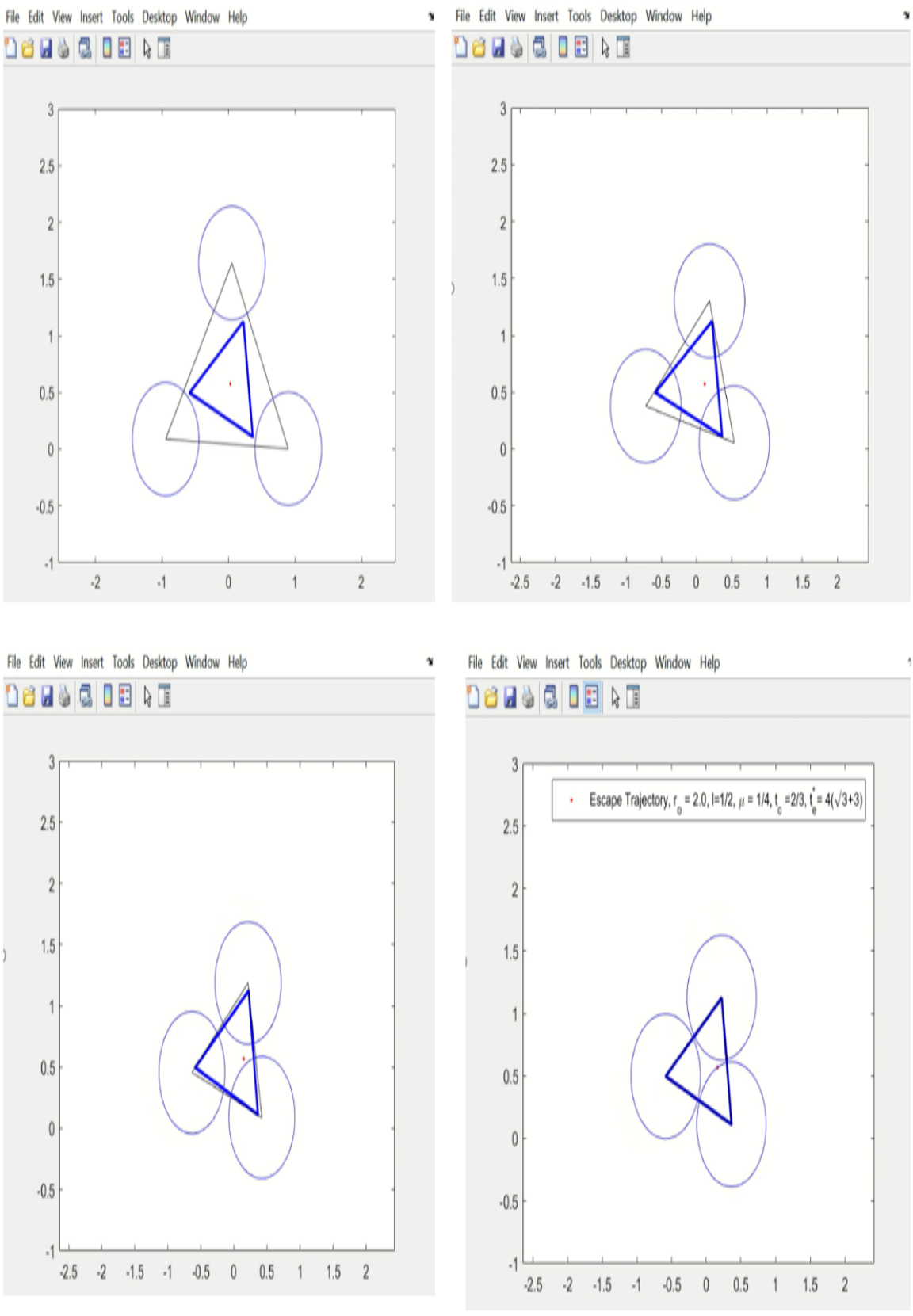


Figure 40: Equidistant pursuers: escape Trajectory, $\mu = \frac{1}{4}, r_o = 2.0, l = 1/2$

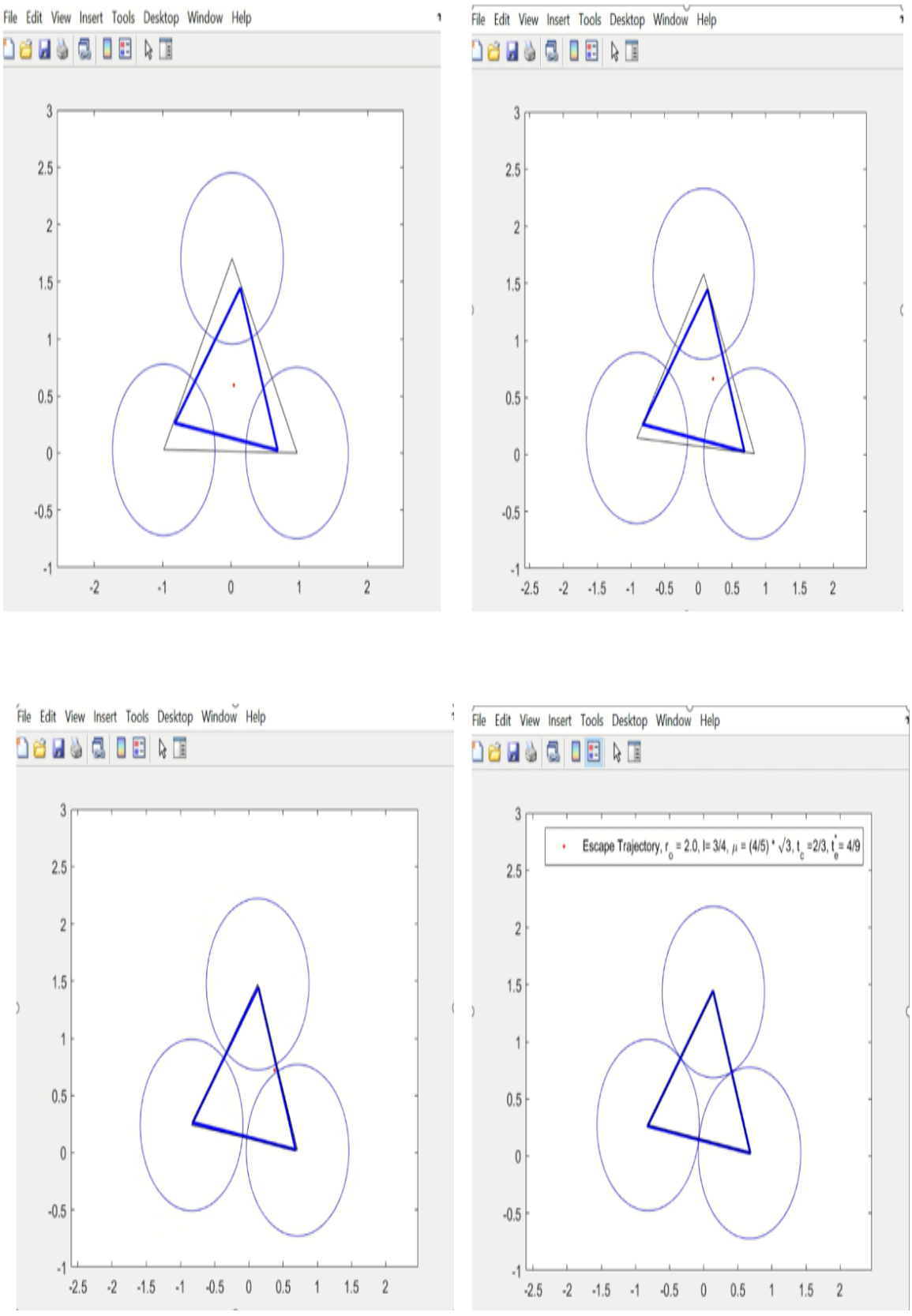


Figure 41: Equidistant pursuers: escape Trajectory, $\mu = \frac{4}{5}\sqrt{3}, r_o = 2.0, l = 3/4$

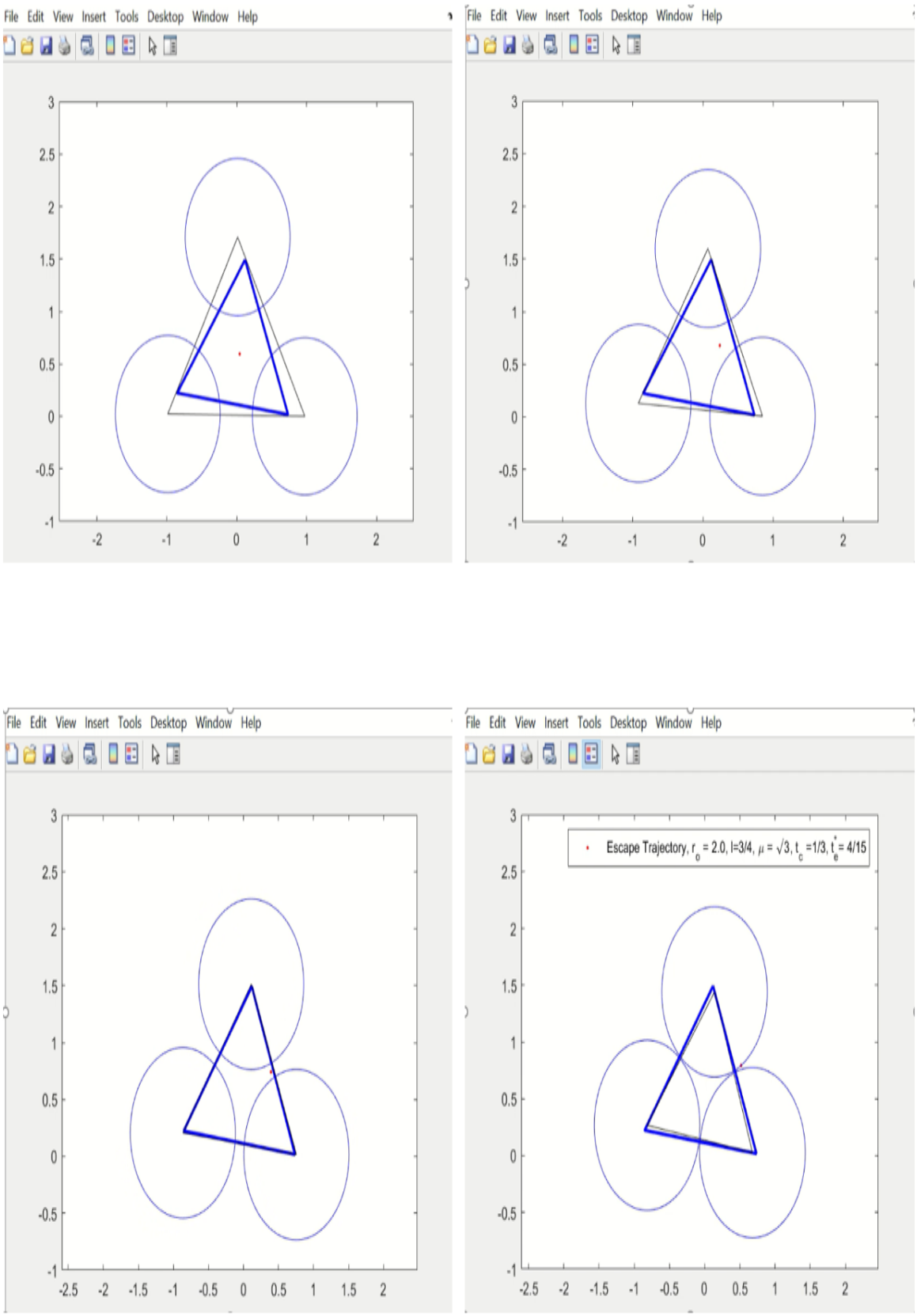


Figure 42: Equidistant pursuers: escape Trajectory, $\mu = \sqrt{3}, r_o = 2.0, l = 3/4$

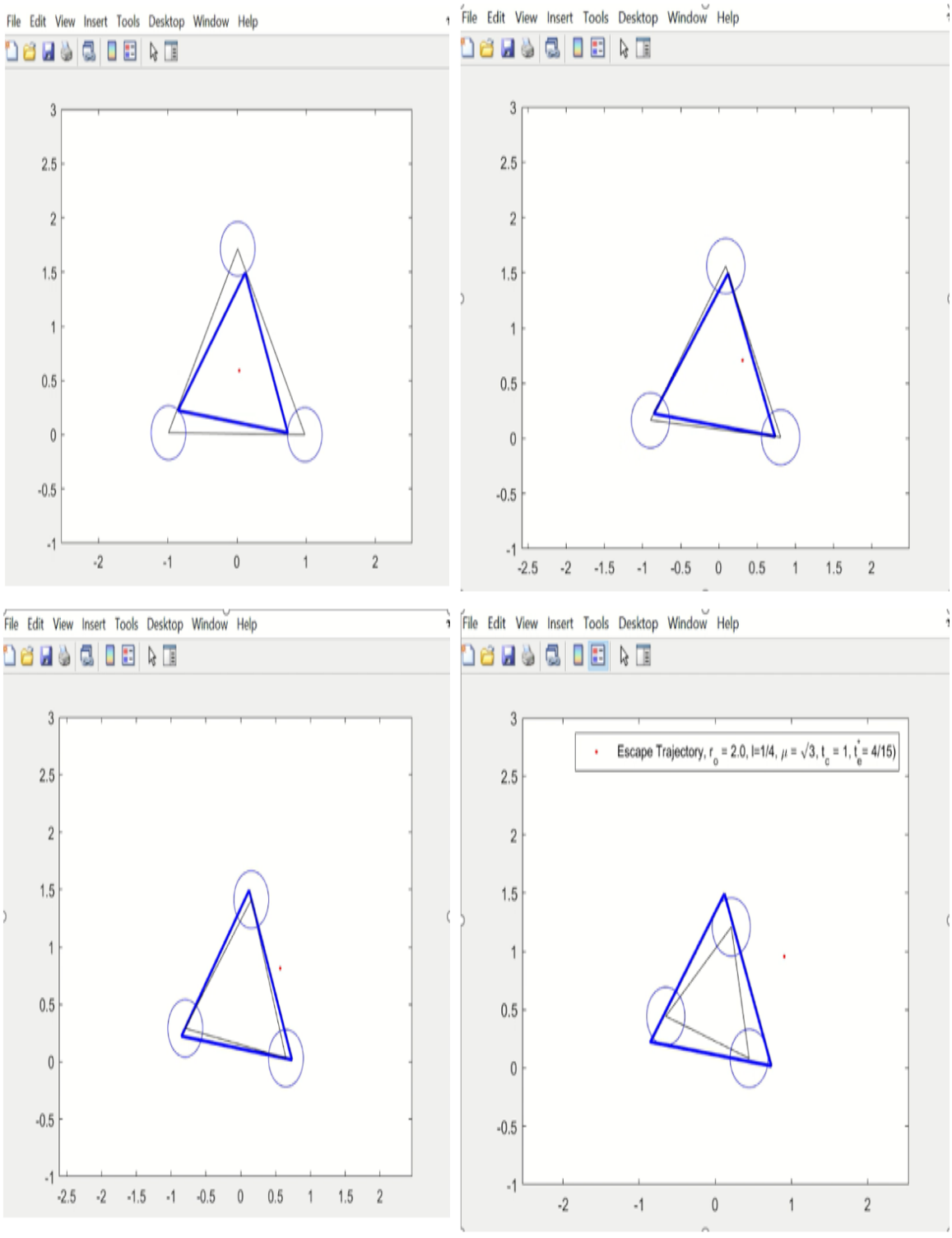


Figure 43: Equidistant pursuers: escape Trajectory, $\mu = \sqrt{3}, r_o = 2.0, l = 1/4$

# V. Conclusions

In this thesis we explored cyclic pursuit involving three pursuers and one evader. We explored evader evading by a predetermined direction and dynamically by choosing the route of the midpoint of the escape cone with the biggest angle. We also studied the outcome of moving the evader away from the center of the encirclement by the pursuers but onto a circumference of circle which is centered in the midpoint of the encirclement. Several simulations were conducted to measure the time of capture for these scenarios while varying evader speed, evaders location on the circumference of the circle and the pursuers capture ranges. Regarding capture, we confirmed for all cases that low evader speed and high pursuer capture range were instrumental to success.

The temporal evolution of the length of distances between the pursuers was studied. By analyzing the plots generated, the determination was made that the evolution of lengths behaved differently based on whether the lengths were the same or not. In the non-equidistant formation scenario, a proposition was made which contained a few requirements. Those requirements were confirmed through simulation results. It was proposed that during the evolution there will be many times in which two of the three distances would be equal for a fleeting moment. It was also proposed the two of the three pursuers would eventually come together and proceed to head on collision towards the third pursuer as a way of then eventually coming together. However, for the equidistant formation scenario the evolution would be simply an equal rate of decline for all the distances. All three pursuers would eventually coalesce at the center of the formation and would do so at the same time. Seveal plots of the trajectories formed were analyzed in this process.

Regarding the study on the shrinking formations : for the non-equidistant scenario, it resulted in a straight line in the innermost triangle emblematic of the train wreck

scenario. For the equilateral triangle, all three pursuers coalesced to the center at the same time leading to a shrinking triangle also resulting in the 'dot' in the center of the innermost triangle.

Finally, regarding the n-gon polygon formation, two finding were discovered. For the irregular n-gons which has no sides the same length, their formation reduced to n-1 gons repeatedly until two cluster remained which eventually coalesced. Regular n-gons formations maintained their symmetry until convergence.

Lastly by applying algebraic principles for a triangle formation for given radius $r_o$ and pursuer capture range $l$, equations were derived to predict capturability. The equations were validated by testing several scenarios by simulation in MATLAB. The goal of this research was to develop strategies from the findings. Based on what has been itemized above, in the analysis of this thesis, for a better probability of capture, an increase in the pursuer's capture range was beneficial. For a regular n-gon formation, the formation remains an n-gon all the way to the end. For an irregular n-gon, the formation collapses and the evader can find itself outside of the formation. A regular formation of swarm attackers is recommended to give a better chance of capture.

## 5.1 Future Work

- Research can be done to allow for pursuers of varied individual speeds to see how it affects the evaders' chances of escape

# Bibliography


1. Tae Hyoung Kim and Toshiharu Sugie. Cooperative control for target-capturing task based on a cyclic pursuit strategy. Automatica, 43(8):1426–1431, 2007.

2. Dwaipayan Mukherjee, Minh Hoang Trinh, Daniel Zelazo, and Hyo Sung Ahn. Bearing-only cyclic pursuit in 2-D for capture of moving target. 57th Isr. Annu. Conf. Aerosp. Sci. IACAS 2017, pages 1–16, 2017.

3. Shaunak D. Bopardikar, Francesco Bullo, and João P. Hespanha. On discrete-time pursuit-evasion games with sensing limitations. IEEE Trans. Robot., 24(6):1429–1439, 2008.

4. Shinji Hara, Tae Hyoung Kim, and Yutaka Hori. Distributed formation control for target-enclosing operations based on a cyclic pursuit strategy. In IFAC Proc. Vol., volume 17, 2008.

5. Kevin S. Galloway, Eric W. Justh, and P. S. Krishnaprasad. Symmetry and reduction in collectives: Cyclic pursuit strategies. Proc. R. Soc. A Math. Phys. Eng. Sci., 469(2158), oct 2013.

6. Cumrun Vafa. Puzzles to Unravel the Universe. Independently published, USA, 2020.

7. Huixin Yang, Tao Yang, and Weihua Zhang. Review on cyclic pursuit in Spacecraft Formation Flying. In RAST 2011 - Proc. 5th Int. Conf. Recent Adv. Sp. Technol., pages 576–580, 2011.

8. Balaji R. Sharma, Subramanian Ramakrishnan, and Manish Kumar. Perimeter tracking by multiple UAVs based on a cyclic-pursuit algorithm. In AIAA Infotech

Aerosp. (I A) Conf. American Institute of Aeronautics and Astronautics Inc., 2013.

9. Geoffrey Hollinger, Sanjiv Singh, Joseph Djugash, and Athanasios Kehagias. Efficient multi-robot search for a moving target. Int. J. Rob. Res., 28(2):201–219, feb 2009.

10. K. S. Galloway, E. W. Justh, and P. S. Krishnaprasad. Geometry of cyclic pursuit. In Proc. IEEE Conf. Decis. Control, pages 7485–7490, 2009.

11. Hu Min and Zeng Guoqiang. Application of Cyclic Pursuit Strategy to Formation Reconfiguration of Spacecraft Clusters. Technical report, 2012.

12. Arpita Sinha and Debasish Ghose. Generalization of linear cyclic pursuit with application to rendezvous of multiple autonomous agents. IEEE Trans. Automat. Contr., 51(11):1819–1824, nov 2006.

13. Jyh Ching Juang. On the formation patterns under generalized cyclic pursuit. IEEE Trans. Automat. Contr., 58(9):2401–2405, 2013.

14. Zhiyun Lin, Mireille Broucke, and Bruce Francis. Local control strategies for groups of mobile autonomous agents. IEEE Trans. Automat. Contr., 49(4):622–629, apr 2004.

15. A. Sinha and D. Ghose. Generalization of the cyclic pursuit problem. In Proc. Am. Control Conf., volume 7, pages 4997–5002, 2005.

# REPORT DOCUMENTATION PAGE

*Form Approved*
*OMB No. 0704–0188*



| 1. REPORT DATE *(DD–MM–YYYY)* | 2. REPORT TYPE | 3. DATES COVERED *(From — To)* |
|---|---|---|
| 25–03–2021 | Master's Thesis | Sept 2019 — Mar 2021 |

**4. TITLE AND SUBTITLE**

Cyclic Pursuit

**5a. CONTRACT NUMBER**

**5b. GRANT NUMBER**

**5c. PROGRAM ELEMENT NUMBER**

**6. AUTHOR(S)**

Oke, Daniel E, TSgt, USAF

**5d. PROJECT NUMBER**

**5e. TASK NUMBER**

**5f. WORK UNIT NUMBER**

**7. PERFORMING ORGANIZATION NAME(S) AND ADDRESS(ES)**

Air Force Institute of Technology
Graduate School of Engineering and Management (AFIT/EN)
2950 Hobson Way
WPAFB OH 45433-7765

**8. PERFORMING ORGANIZATION REPORT NUMBER**

AFIT-ENG-MS-21-M-068

**9. SPONSORING / MONITORING AGENCY NAME(S) AND ADDRESS(ES)**

Control System Science
2210 8th ST Building 20146 Rm 300
WPAFB OH 45433-7765
DSN 713-7373, COMM 937-255-8495
Email: david.casbeer@us.af.mil

**10. SPONSOR/MONITOR'S ACRONYM(S)**

AFRL/RQ

**11. SPONSOR/MONITOR'S REPORT NUMBER(S)**

**12. DISTRIBUTION / AVAILABILITY STATEMENT**

DISTRIBUTION STATEMENT A:
APPROVED FOR PUBLIC RELEASE; DISTRIBUTION UNLIMITED

**13. SUPPLEMENTARY NOTES**

This work is declared a work of the U.S. Government and is not subject to copyright protection in the United States.

**14. ABSTRACT**

This thesis analyzes cyclic pursuit with the intent of developing swarm attack strategies for autonomous agents. Research was focused on finding the effects of pursuers capture range, evader speed and size of formation on the probability of escape. The temporal evolution of several polygonal formations was analyzed. The polygons could be regular or arbitrary polygons. The thesis demonstrated that an increased capture range, formation size, reduced evader speed aided capture probability. Irregular n-gon formations reduced to n-1 gon repeatedly, pursuer clusters formed until two clusters remained which eventually came together, so all the n pursuers coalesced until convergence. Regular n-gon polygon formation maintained their form until coalesced. Sufficient conditions for the capture of the evader are provided at the end of the analysis.

**15. SUBJECT TERMS**

Capture range, Capturability, Polygon Formation Evolution

| 16. SECURITY CLASSIFICATION OF: | | | 17. LIMITATION OF ABSTRACT | 18. NUMBER OF PAGES | 19a. NAME OF RESPONSIBLE PERSON |
|---|---|---|---|---|---|
| a. REPORT | b. ABSTRACT | c. THIS PAGE | | | Dr. Meir Pachter, AFIT/ENG |
| U | U | U | UU | 89 | 19b. TELEPHONE NUMBER *(include area code)* (937) 255-3636, ext 7247; meir.pachter@afit.edu |